The Plant Cell, Vol. 27: 1140–1161, April 2015, www.plantcell.org

Arabidopsis RIC1 Severs Actin Filaments at the Apex to Regulate Pollen Tube Growth

Zhenzhen Zhou,[a,1] Haifan Shi,[a,1] Binqing Chen,[a,1] Ruihui Zhang,[b] Shanjin Huang,[b] and Ying Fu[a,2]

[a] State Key Laboratory of Plant Physiology and Biochemistry, College of Biological Sciences, China Agricultural University, Beijing 100193, China

[b] Key Laboratory of Plant Molecular Physiology, Institute of Botany, Chinese Academy of Sciences, Beijing 100093, China

Pollen tubes deliver sperms to the ovule for fertilization via tip growth. The rapid turnover of F-actin in pollen tube tips plays an important role in this process. In this study, we demonstrate that *Arabidopsis thaliana* RIC1, a member of the ROP-interactive CRIB motif-containing protein family, regulates pollen tube growth via its F-actin severing activity. Knockout of *RIC1* enhanced pollen tube elongation, while overexpression of *RIC1* dramatically reduced tube growth. Pharmacological analysis indicated that RIC1 affected F-actin dynamics in pollen tubes. In vitro biochemical assays revealed that RIC1 directly bound and severed F-actin in the presence of Ca^{2+} in addition to interfering with F-actin turnover by capping F-actin at the barbed ends. In vivo, RIC1 localized primarily to the apical plasma membrane (PM) of pollen tubes. The level of RIC1 at the apical PM oscillated during pollen tube growth. The frequency of F-actin severing at the apex was notably decreased in *ric1-1* pollen tubes but was increased in pollen tubes overexpressing RIC1. We propose that RIC1 regulates F-actin dynamics at the apical PM as well as the cytosol by severing F-actin and capping the barbed ends in the cytoplasm, establishing a novel mechanism that underlies the regulation of pollen tube growth.

INTRODUCTION

After pollen grain germination on the stigma of a flowering plant, the pollen tube undergoes an extreme form of polarized growth, termed tip growth, which drives extension of the pollen tube into the style and delivers two sperms to the ovule for fertilization. It is well established that the actin cytoskeleton is an important regulator of pollen tube tip growth. F-actin is organized into distinct arrays in different regions of the pollen tube. Using Lifeact-mEGFP or fluorescently tagged actin binding proteins (ABPs) or their actin binding domains as probes, apical F-actin was revealed to be highly dynamic in pollen tubes (Cheung et al., 2008; Kost, 2008; Vidali et al., 2009). Subsequent studies demonstrated that this highly dynamic F-actin pool is generated from the apical and subapical plasma membrane (PM) (Cheung et al., 2010; Qu et al., 2013).

During pollen tube tip growth, the organization and dynamics of different actin structures are directly regulated by several classes of ABPs (Ren and Xiang, 2007; Staiger et al., 2010). Signaling pathways that modulate pollen tube tip growth have been found to transmit signals to these ABPs, thereby regulating the organization of F-actin arrays and the rapid turnover of F-actin. The roles of profilins, formins, ADFs, and capping proteins in the regulation of subapical and apical F-actin structures have long been appreciated (Ren and Xiang, 2007; Cheung and Wu, 2008; Staiger et al., 2010). For example, Cheung et al. (2010) showed that the apical dome-localized Formin Homology5 (FH5) protein was a membrane-anchored actin-nucleating protein that stimulated actin assembly in the tip regions of pollen tubes. A role for calcium-dependent villins in the regulation of apical F-actin dynamics in pollen tubes has also been demonstrated (Yokota et al., 2005; Zhang et al., 2010; Qu et al., 2013). VILLIN2 (VLN2) and VLN5 were shown to promote actin turnover at pollen tube tips and to facilitate the construction of actin collars (also referred to as the actin fringe) via F-actin severing in response to calcium signaling (Qu et al., 2013). Interestingly, several bifunctional microtubule-associated proteins (MAPs) also exhibit F-actin binding activity. In *Solanum berthaultii*, SB401 was found to bind both microtubules and F-actin in vitro (Huang et al., 2007). *Arabidopsis thaliana* MAP18, a microtubule-destabilizing factor that modulates polarized cell growth in vegetative tissues (Wang et al., 2007), was recently demonstrated to regulate the direction of pollen tube growth via its Ca^{2+}-dependent F-actin severing activity (Zhu et al., 2013). VLN2, VLN5, and MAP18 were shown to sever F-actin in the cytoplasm at the tip of the pollen tube (Qu et al., 2013; Zhu et al., 2013), where a tip-focused Ca^{2+} gradient is present. Qu et al. (2013) proposed that VLN2 and VLN5 sever F-actin originating from the apical PM to facilitate its subsequent use in the construction of the actin collars/fringe. However, the F-actin disassembly/severing activities of these ABPs were reported to take place in the cytosol, and the precise mechanism by which PM-anchored F-actin is released/disassociated from the apical/subapical PM remains unknown.

Cortical F-actin has been suggested to be required for vesicle targeting, but it has also been shown to block vesicle docking and fusion to the target PM (Gu et al., 2005; Lee et al., 2008; Kroeger et al., 2009). Therefore, these results suggest that both F-actin assembly and disassembly are required for normal tip growth and must be properly regulated. ROP (Rho-like GTPase of plants)-dependent signaling pathways play pivotal roles in the

[1] These authors contributed equally to this work.

[2] Address correspondence to yingfu@cau.edu.cn.

The author responsible for distribution of materials integral to the findings presented in this article in accordance with the policy described in the Instructions for Authors (www.plantcell.org) is: Ying Fu (yingfu@cau.edu.cn)

www.plantcell.org/cgi/doi/10.1105/tpc.114.135400

modulation of F-actin dynamics during pollen tube tip growth (Smith and Oppenheimer, 2005; Hussey et al., 2006; Cheung and Wu, 2008; Yalovsky et al., 2008; Qin and Yang, 2011). Arabidopsis ROP1 was found to be preferentially activated and localized to the apical PM of pollen tubes. ROP1 was shown to regulate pollen tube tip growth by activating two counteracting downstream pathways mediated by RIC3 (Rop-interactive CRIB motif-containing protein3) and RIC4, respectively. RIC4 promotes F-actin assembly, and RIC3 promotes F-actin disassembly through promoting the formation of a Ca^{2+} gradient at the tip (Gu et al., 2005; Lee et al., 2008).

RIC1 is another member of the RIC protein family (Wu et al., 2001). Our previous study in leaf pavement cells revealed that RIC1 is a microtubule-associated protein that can be activated by ROP6 to reorder microtubules by promoting the microtubule severing activity of katanin (Fu et al., 2005, 2009; Lin et al., 2013). Interestingly, Lin et al. (2012) recently suggested that an auxin-activated ROP6-RIC1 pathway inhibits PIN-FORMED2 (PIN2) internalization by stabilizing F-actin in root cells, indicating that RIC1 may function differently in various cell types by modulating either microtubules or F-actin. In addition, microarray analysis indicates that RIC1 is highly expressed in pollen grains (https://www.genevestigator.com), potentially implicating RIC1 in pollen and/or pollen tube growth.

In this study, we have demonstrated that RIC1 regulates pollen tube growth through its F-actin severing and capping activities. We propose that the severing activity of PM-localized RIC1 helps to release F-actin from the apical/subapical PM into the cytoplasm. Additionally, RIC1 also severs F-actin in the cytoplasm of the pollen tube tip and then caps the barbed ends of the F-actin fragments to prevent further elongation. Our results demonstrate that RIC1 contributes to the dynamics and abundance of F-actin in the apices and subapices of pollen tubes, thereby regulating pollen tube growth.

RESULTS

RIC1 Is Highly Expressed in Arabidopsis Pollen Tubes

Data extracted from the results of Affymetrix AG and ATH1 GeneChip arrays (www.genevestigator.ethz.ch) indicate that *RIC1* is highly expressed in the Arabidopsis flower, particularly in mature pollen (Supplemental Figure 1A). To further assess the expression of RIC1 in Arabidopsis plants, we fused the *RIC1* promoter (2-kb DNA upstream of ATG) to the β-glucuronidase (GUS) reporter gene and introduced the resulting construct into wild-type Columbia-0 (Col-0) plants. Five independent T3 lines were used for GUS activity analysis. Consistent with previously reported RT-PCR and GUS analysis results (Wu et al., 2001; Choi et al., 2013) and microarray data, GUS activity was detected in various organs, including cotyledons, hypocotyls, roots, leaves, and flowers, but *RIC1* was expressed at the highest levels in stamens and mature pollen grains. In addition, *RIC1* promoter activity was also detected at high levels in germinated pollen tubes in vitro (Supplemental Figure 1). Together, these data suggest that RIC1 may play a role in pollen germination and pollen tube growth.

RIC1 Negatively Affects Pollen Tube Growth

To investigate the role of RIC1 in pollen germination and pollen tube growth, we collected pollen grains from Wassilewskija-2 (Ws-2) plants harboring *ric1-1*, a null allele that lacks the expression of detectable full-length *RIC1* cDNA in the flower (Figure 1A). Pollen grains were germinated in vitro. The number of germinated pollen grains was counted, and germination frequency was quantified as a percentage (Boavida and McCormick, 2007). At 1 h after germination, the average pollen germination frequency of control Ws-2 plants was 46% ± 1% (mean ± SE), while that of *ric1-1* was 56% ± 2%, indicating that loss of RIC1 resulted in a significant increase in germination frequency at this time point ($P < 0.05$, Student's *t* test). However, there was no significant difference in the average germination frequency of wild-type (72% ± 2%) and *ric1-1* (75% ± 2%) pollen grains at 1.5 h after germination (Figure 1B). This observation suggests that emergence of the tube occurs faster in the *ric1-1* mutant, but eventually there is no significant difference in germination frequency between the *ric1-1* and wild-type pollen.

We compared the mean lengths of wild-type and *ric1-1* pollen tubes at 1.5, 3, and 5 h after germination in vitro. *ric1-1* pollen tubes were significantly longer than those in wild-type plants (Figures 1C and 1D). These results demonstrate that loss of RIC1 function resulted in an increase in pollen tube length.

To determine whether longer *ric1-1* pollen tubes were the result of more rapid germination of *ric1-1* pollen or faster growing *ric1-1* pollen tubes, individual tubes that had been grown on the germination medium for 2 to 4 h were monitored by light microscopy for 5 min. The average growth rate of wild-type pollen tubes was 2.38 ± 0.09 μm/min compared with 2.84 ± 0.08 μm/min for *ric1-1* pollen tubes. The average growth rate of *ric1-1* pollen tubes was significantly higher than that of wild-type pollen tubes (Figures 1E and 1F; $P < 0.01$, Student's *t* test).

To confirm that RIC1 plays a role in pollen tube elongation, a complementation experiment was performed. *RIC1-GFP* was expressed under the control of its native promoter in *ric1-1* plants. Eight transgenic lines (*COM 1*, *COM 3*, *COM 5*, *COM 6*, *COM 7*, *COM 8*, *COM 11*, and *COM 12*) were found to exhibit various *RIC1* expression levels by RT-PCR analysis (Figure 1A), and four lines (*COM 1*, *COM 5*, *COM 6*, and *COM 11*) had *RIC1* expression levels similar to that of wild-type Ws-2 plants. We used *COM 11* for further phenotypic analysis. The faster germination and enhanced pollen tube elongation phenotypes caused by knocking out of RIC1 were fully recovered in *COM 11* (Figures 1B to 1F), demonstrating that *RIC1* is responsible for the phenotype and that the green fluorescent protein (GFP) tag does not affect RIC1 function.

To assess the effects of RIC1 overexpression, we generated five additional transgenic lines in the Col-0 background that stably overexpressed *RIC1* under the control of the Lat52 promoter. Two of these lines (named *OX 9* and *OX 15*; Figure 1G) were used for further analysis. Real-time quantitative RT-PCR (qRT-PCR) revealed that expression of *RIC1* in the *RIC1 OX 9* and *OX 15* lines was ~2.5-fold higher than that of the Col-0 line (Figure 1H). Dramatic inhibition of pollen germination and pollen tube elongation was observed in these overexpression lines (Figures 1G, 1I, and 1J).

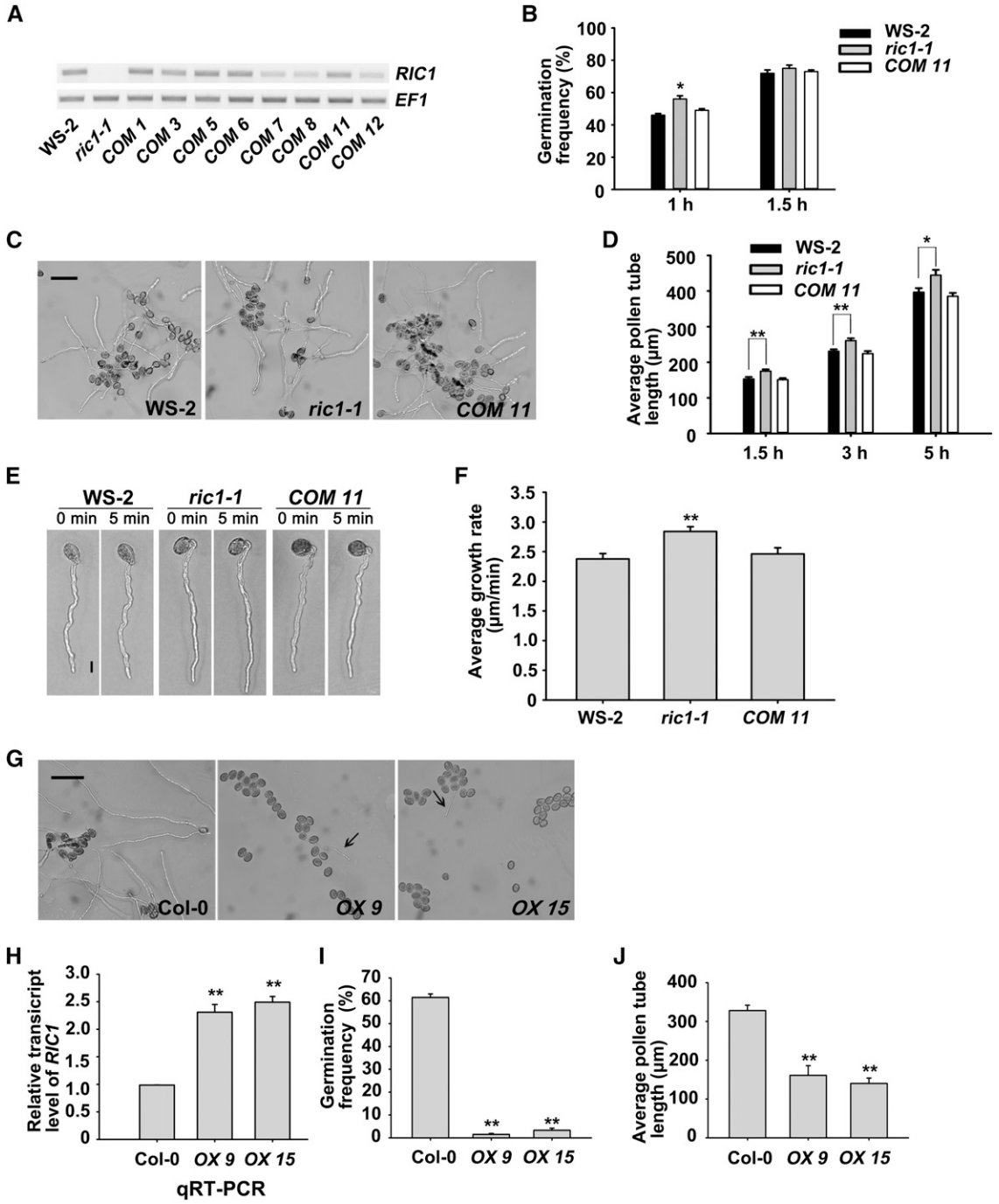

Figure 1. RIC1 Regulates Pollen Tube Germination and Growth.

All data are presented as means ± SE. *P < 0.05, **P < 0.01, by Student's *t* test.

(A) *COM 1*, *COM 3*, *COM 5*, *COM 6*, *COM 7*, *COM 8*, *COM 11*, and *COM 12* are transgenic lines generated by transforming *ProRIC1:RIC1-GFP* into *ric1-1* plants. RT-PCR analysis demonstrated that *ric1-1* is a null loss-of-function mutant and that RIC1 expression levels in *COM 1*, *COM 5*, *COM 6*, and *COM 11* lines were similar to levels in wild-type (Ws-2) plants. *EF1αA4* (*EF1*) served as an internal control. This result is representative of three replicates conducted on three biologically independent samples.

(B) The germination frequency of Ws-2, *ric1-1*, and *COM 11* pollen was analyzed at 1 and 1.5 h after the initiation of germination. The germination frequency of *COM 11* pollen was similar to that of Ws-2 pollen at each time point. A larger number of *ric1-1* pollen grains germinated compared with wild-type pollen at 1 h after initiation. No significant difference was detected at 1.5 h after initiation. About 1000 pollen grains from three independent experiments were analyzed.

To test whether RIC1 overexpression affects pollen germination and pollen tube growth in vivo, pollen grains from wild-type (Col-0) and *RIC1 OX 9* plants were used to pollinate wild-type stigma, followed by staining with aniline blue at various time points after pollination. As shown in Supplemental Figures 2A to 2F, pollen germination and pollen tube growth were severely reduced in *RIC1 OX* plants.

By contrast, comparison of *ric1-1* and wild-type Ws-2 pollen tube growth at various time points revealed no overt differences between the two lines (Supplemental Figures 2G to 2L). However, due to difficulty in accurately measuring the length of each individual pollen tube in vivo, subtle differences may be hard to discern. Together, these results suggest that RIC1 is involved in the negative regulation of pollen germination and pollen tube growth in vivo.

RIC1 Regulates Apical Actin Filaments in Pollen Tubes

Previous studies demonstrated that RIC1 is a microtubule-associated protein that is activated by ROP6 to promote the microtubule ordering in leaf pavement cells (Fu et al., 2005, 2009). Because F-actin is critically important for pollen tube tip growth and ROP1-mediated signaling pathways regulate F-actin dynamics to regulate the polar growth of pollen tubes (Kost, 2008; Qin and Yang, 2011), we hypothesized that RIC1, a known downstream effector of ROP GTPases, might regulate F-actin in pollen tubes.

To determine whether microtubules are required for the function of RIC1 in pollen tube growth, we treated *ric1-1* and Ws-2 pollen tubes with oryzalin, a microtubule-disrupting drug. The relative average lengths (treated tubes versus control tubes) of in vitro-germinated pollen tubes were not significantly different between *ric1-1* and wild-type pollen in the presence of various concentrations of oryzalin in the germination medium (Figure 2A). This observation is consistent with previous studies reporting that although 1 μM oryzalin efficiently disturbed microtubules in pollen tubes, pollen tube growth was unaffected (Gossot and Geitmann, 2007; Bou Daher and Geitmann, 2011). Further observation of the microtubule cytoskeleton in pollen tubes by immunostaining revealed no overt differences in microtubule organization between *ric1-1* and Ws-2 pollen tubes (Supplemental Figure 3).

To assess the role of actin in RIC1-dependent pollen tube growth, we applied a low concentration (1 nM) of latrunculin B (LatB), an F-actin depolymerizing drug, to the germination medium. In previous studies, low concentrations of LatB were reported to disturb apical fine F-actin structures but not F-actin cables in the shanks of pollen tubes (Gibbon et al., 1999; Hwang et al., 2008). Results from this analysis showed that 1 nM LatB reduced the growth of both Ws-2 and *ric1-1* pollen tubes (Figure 2B). However, the growth of Ws-2 pollen tubes was significantly more affected than that of *ric1-1* pollen tubes in the presence of 1 nM LatB (Figure 2B). These observations suggest that RIC1 may regulate F-actin, but not microtubules, to affect pollen tube growth. Interestingly, the average lengths of treated Col-0 wild-type and *OX 9* pollen tubes were reduced to 80% ± 3% and 76% ± 4%, respectively, of each untreated control (Figure 2B). Perhaps the growth of pollen tubes had already been severely inhibited by overexpressing RIC1 (Figures 1G and 1J) and the apical fine F-actin had been dramatically disturbed (see below). Therefore, *OX 9* pollen tubes are not hypersensitive to 1 nM LatB compared with wild-type tubes.

We next observed F-actin organization in control, *ric1-1*, and *RIC1 OX 9* pollen tubes using Lifeact-mEGFP. We first verified that RIC1 did not affect the affinity of Lifeact-mEGFP for F-actin using an in vitro cosedimentation assay (Supplemental Figure 4A). Because the *Lifeact-mEGFP* marker line was in the Col-0 background, we crossed the *ric1-1* line with Col-0 three times to replace the background before crossing the *ric1-1 (Col-0)* line with the *Lifeact-mEGFP* marker line to visualize F-actin organization and dynamics in pollen tubes. We compared the growth rates of Col-0 pollen tubes expressing *Lifeact-mEGFP* and *ric1-1 (Col-0)* pollen tubes expressing *Lifeact-mEGFP*. Similar to our observations in Ws-2 and *ric1-1* pollen tubes, *ric1-1 (Col-0)* pollen tubes exhibited a faster growth rate (3.59 ± 0.11 μm/min; $n = 25$) than Col-0 pollen tubes (3.29 ± 0.10 μm/min; $n = 24$). Using Lifeact-mEGFP, three distinct actin structures were observed from the apical to shank regions, as shown in Figure 2D, Supplemental

Figure 1. (continued).

(C) In vitro-germinated pollen tubes from Ws-2, *ric1-1*, and *COM 11* pollen at 3 h after germination. Bar = 100 μm.

(D) The average pollen tube lengths of Ws-2, *ric1-1*, and *COM 11* pollen (only germinated pollen grains were taken into account) were analyzed at 1.5, 3, and 5 h after germination. Pollen tubes from *ric1-1* pollen were consistently longer than those of wild-type pollen. The average pollen tube length of *COM 11* was similar to Ws-2 at each time point (~300 pollen tubes per data set).

(E) Representative Ws-2, *ric1-1*, and *COM 11* pollen tubes were tracked for 5 min at 2 h after the initiation of germination. The *ric1-1* pollen tube grew faster than the Ws-2 and *COM 11* tubes. Bar = 10 μm.

(F) Pollen tube growth rates were quantitatively analyzed by tracking individual pollen tubes at 2 to 4 h after the initiation of germination for 5 min. The average growth rate of *ric1-1* tubes was higher than that of Ws-2 tubes. However, there was no significant difference between Ws-2 and *COM 11* tubes ($n > 70$ pollen tubes per data set).

(G) Pollen tubes from wild-type (Col-0) and *RIC1 OX* (*OX 9* and *OX 15*) pollen were observed at 5 h after germination. Overexpression of RIC1 dramatically inhibited pollen germination. Arrows indicate germinated pollen tubes. Bar = 100 μm.

(H) Quantitative real-time PCR analysis showed that the expression of *RIC1* is ~2.5-fold higher in *RIC1 OX 9* and *OX 15* plants compared with wild-type plants.

(I) and **(J)** The average germination frequency **(I)** and pollen tube length **(J)** of Col-0 and *RIC1 OX* pollen were analyzed 5 h after germination. Overexpression of RIC1 significantly reduced pollen germination as well as pollen tube elongation. Approximately 1000 pollen grains were analyzed to calculate the pollen germination frequency of wild-type and *RIC1 OX* pollens **(I)**, and ~200 Col-0 and 30 *RIC1 OX* pollen tubes were measured for pollen tube length experiments **(J)**.

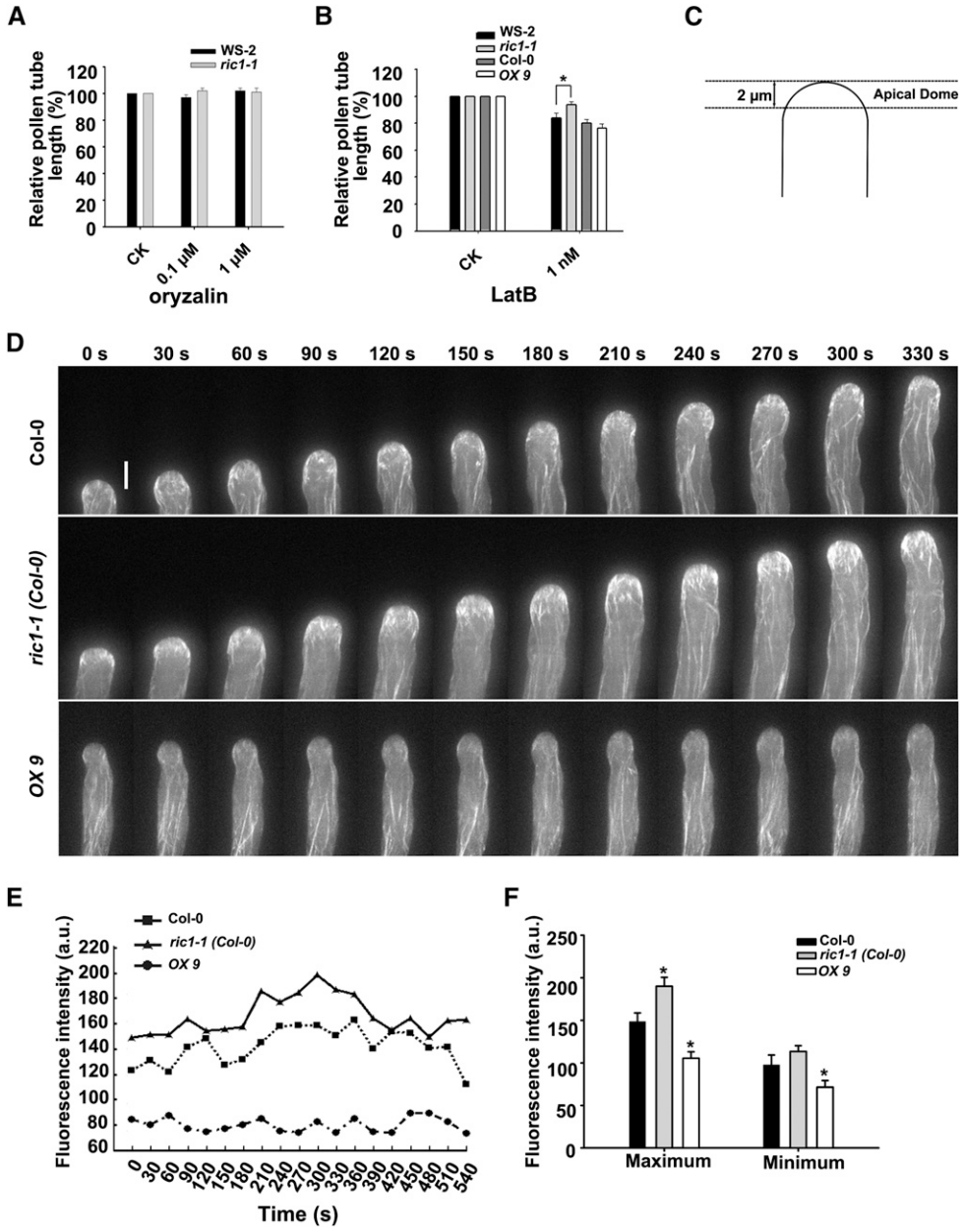

Figure 2. RIC1 Acts on Apical Actin Filaments in Pollen Tubes.

All data are presented as means ± SE. *P < 0.05, by Student's *t* test.

(A) Ws-2 and *ric1-1* pollen tubes were incubated on germination medium containing different concentrations of oryzalin. The average lengths of treated pollen tubes relative to untreated controls at 3 h after germination were calculated. Untreated controls were normalized to 100% for Ws-2 and *ric1-1* pollen. Oryzalin had little effect on pollen tube growth. CK, untreated control.

(B) Ws-2, *ric1-1*, Col-0, and *OX 9* pollen tubes were incubated on germination medium containing 1 nM LatB. The average lengths of treated pollen tubes relative to untreated controls at 3 h after germination were calculated. Untreated controls were normalized to 100% for pollen from each line. *ric1-1* pollen tubes were more resistant to LatB than wild-type (Ws-2) tubes, whereas there was no significant difference between *OX 9* and Col-0 pollen tubes.

(C) Schematic showing how the apical dome zone in the pollen tube was defined. A semielliptical region circumscribed by the dotted line at the tip was selected for the apical F-actin analyses shown in **(D)**.

(D) Time-lapse images from Supplemental Movie 1 (Col-0), Supplemental Movie 2 [*ric1-1 (Col-0)*], and Supplemental Movie 3 (*RIC1 OX 9*) showing F-actin dynamics in growing pollen tubes. Bar = 5 μm.

Movie 1, Supplemental Figure 4B, and previous reports (Qu et al., 2013; Zhu et al., 2013). Highly dynamic fine F-actin structures were observed at the apices, abundant and dense F-actin structures were present at the subapical regions, and parallel longitudinally orientated F-actin cables were found at the shank regions in Col-0, *RIC1 OX 9*, and *ric1-1 (Col-0)* pollen tubes. In the shank region, no obvious differences were detected between Col-0 and *ric1-1 (Col-0)* pollen tubes in terms of F-actin abundance or bundling (Supplemental Figures 5A and 5B). Although an increase in filament density and F-actin bundling was displayed in the shank region of *RIC1 OX 9* pollen tubes (Supplemental Figures 5A and 5B), this was likely caused by RIC1 overexpression as opposed to an actual function of RIC1, since RIC1 was primarily localized to the apical PM in pollen tubes (Figure 3; Supplemental Figure 6).

In the tip region, no significant difference was detected between wild-type and *ric1-1 (Col-0)* pollen tubes regarding F-actin bundling, suggesting that RIC1 may not have an effect on F-actin bundling in the tip (Supplemental Figure 5D). However, *ric1-1 (Col-0)* pollen tubes displayed an increase in the amount of F-actin, while *RIC1 OX 9* pollen tubes exhibited a decrease within the apical dome compared with the wild type (Supplemental Figures 4B and 5C). To precisely quantify the apical fine F-actin structures in growing pollen tubes, the dynamics of apical F-actin were monitored using a spinning disc confocal microscope, and actin structures were quantified by measuring the fluorescence intensity present in the apical dome (Figures 2C to 2F). Time-lapse, Z-stack images (0.5-μm step size) were captured over a 540-s time period at 30-s intervals. Representative images from Col-0, *ric1-1 (Col-0)*, or *RIC1 OX 9* pollen tubes are shown in Supplemental Movies 1, 2, and 3. Although apical F-actin structures were dynamic and oscillatory in all Col-0, *ric1-1 (Col-0)*, and *RIC1 OX 9* pollen tubes, the abundance and oscillatory amplitude of the structures differed between the lines. Apical F-actin structures in *ric1-1* pollen tubes were more abundant with greater oscillatory amplitude (Figures 2D to 2F). Together, these results demonstrate that loss of *RIC1* results in an increase in abundance and a greater oscillatory amplitude of apical F-actin structures, while overexpression of *RIC1* results in a decrease in abundance and a lower oscillatory amplitude of F-actin structures in the apical regions of pollen tubes.

RIC1 Localizes to the PM of Pollen Tube Tips

To investigate the mechanism by which RIC1 functions in the pollen tube tip region, we assessed RIC1 localization in pollen and growing pollen tubes from *COM 11*-complemented plants expressing RIC1-GFP. In pollen grains before germination, RIC1-GFP was observed in a punctate pattern in the cytoplasm, and no PM localization was detected. However, accumulation of GFP-RIC1 at the PM at the germination site was detected shortly before protrusion of the pollen tube, and RIC1-GFP was localized to the PM in the tip of germinating and elongating pollen tubes (Figure 3; Supplemental Figures 6A and 6B). PM localization of RIC1 was confirmed by staining with FM4-64, a membrane marker, as well as by plasmolysis (Supplemental Figures 6C and 6D). It is also consistent with a previous report by Wu et al. (2001). To further investigate the relationship between RIC1 PM localization and pollen grain germination, the percentage of pollen grains and pollen tubes displaying clear PM localization was analyzed, along with the germination rate. After 15 min of incubation in germination medium, almost no pollen grains had germinated; however, ~6% of pollen grains already displayed PM-localized RIC1-GFP (Supplemental Figure 6B). The percentage of pollen/pollen tubes containing PM-localized RIC1-GFP increased steadily prior to the increase in the germination rate during pollen germination (Supplemental Figure 6B), indicating that RIC1 localized to the PM before pollen germination. To more precisely characterize the temporal dynamics of RIC1 localization to the PM, we monitored 22 pollen grains for 1.5 h at 1-min intervals. Indeed, all 6 germinating pollen grains exhibited polarized PM localization of RIC1-GFP at the germination site before emergence of the pollen tube (Figure 3). These observations suggest that the function of RIC1 in pollen tube growth is associated with its localization to the apical PM. However, as loss of function of RIC1 accelerated pollen germination (Figure 1B), recruitment of RIC1 to the PM is not a requirement for germination but is more likely to play a role in preparation for the subsequent growth of the pollen tube.

RIC1 Binds and Severs Actin Filaments in Vitro

The results described above strongly suggest that RIC1 plays a role in pollen tube growth, most likely through the modulation of F-actin. Therefore, we next analyzed the interaction between RIC1 and F-actin in vitro. We performed high-speed cosedimentation experiments to determine whether RIC1 possessed F-actin binding activity. The resulting supernatants and pellets were analyzed separately using SDS-PAGE (Figure 4A). Results from this assay showed that various concentrations of recombinant RIC1 cosedimented with F-actin and were present in the pellets. RIC1 was not detected in the pellets in the absence of F-actin. RIC1 cosedimented with F-actin in a concentration-dependent manner, and binding of RIC1 to F-actin was saturated at a stoichiometry of ~0.75 mol RIC1/mol G-actin (Figure 4B). To determine the value of the equilibrium K_d, the quantity of RIC1 present in the pellet ($[RIC1]_{bound}$) was plotted as a function

Figure 2. (continued).

(E) Oscillations of fine F-actin in the apical dome were quantified by measuring fluorescence intensity in representative growing Col-0, *ric1-1 (Col-0)*, and *RIC1 OX 9* pollen tubes shown in **(D)**. Compared with Col-0, apical F-actin structures in *ric1-1* pollen tubes were more abundant, while there were fewer apical F-actin structures in *RIC1 OX 9* pollen tubes. a.u., arbitrary units.

(F) Average maximum and minimum fluorescence intensities of F-actin in the apical dome of Col-0 ($n = 20$), *ric1-1 (Col-0)* ($n = 20$), and *RIC1 OX 9* ($n = 10$) pollen tubes. Compared with Col-0, apical F-actin structures in *ric1-1* pollen tubes were more abundant with greater oscillatory amplitude, while there were fewer apical F-actin structures with decreased oscillatory amplitude in *RIC1 OX 9* pollen tubes.

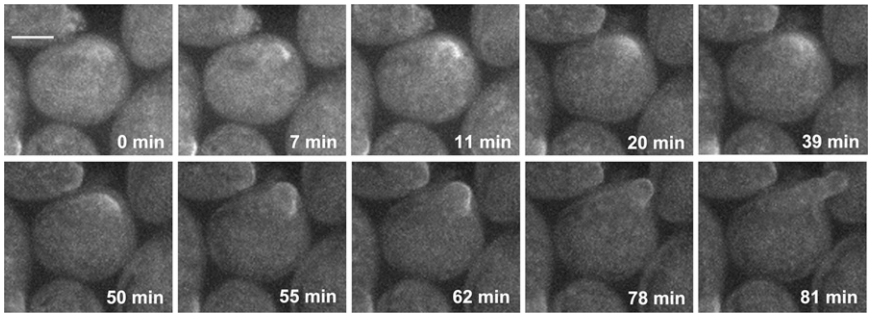

Figure 3. Subcellular Localization of RIC1 Changes during Pollen Tube Germination and Elongation.

Pollen grains from *COM 11* plants (expressing *ProRIC1:RIC1-GFP*) were germinated in vitro and observed using spinning disc confocal microscopy. Before germination, RIC1-GFP was detected in the cytoplasm. RIC1-GFP subsequently localized to the PM at the germination site and was restricted to the PM of the growing pollen tube tip. Images were captured every 1 min for 81 min. Bar = 10 μm.

of the quantity of RIC1 present in the supernatant ($[RIC1]_{free}$), and the resulting data were fitted with a hyperbolic function. In a representative experiment, the K_d value was determined to be 0.76 μM (Figure 4C), and the mean K_d was found to be 0.74 ± 0.08 μM (n = 3).

To further investigate the direct effects of RIC1 on F-actin in vitro, we visualized F-actin using Alexa-488 phalloidin staining with a spinning disc confocal microscope. Preformed F-actin was incubated with 0.5 μM RIC1 for 30 min, followed by staining with Alexa-488 phalloidin (0.5 μM) for an additional 15 min at room temperature, resulting in the formation of massive bundles (Supplemental Figures 7A and 7B). Then, the addition of NaCl, which releases RIC1 from F-actin, resulted in dispersal of the bundles (Supplemental Figure 7C). Results from a low-speed cosedimentation experiment further confirmed that RIC1 bundled F-actin in a concentration-dependent manner (Supplemental Figures 7E and 7F).

Because RIC1 specifically localized to the tip region of the pollen tube, where calcium levels have been shown to be high (Cheung and Wu, 2008; Qin and Yang, 2011), we next tested whether Ca^{2+} affected RIC1-induced F-actin binding or bundling in vitro. Preformed F-actin and RIC1 (2.5 μM) were incubated in the presence of various concentrations of Ca^{2+} prior to high-speed centrifugation. The resulting supernatants and pellets were analyzed by SDS-PAGE. As shown in Supplemental Figure 7G, there were no obvious changes in the amount of RIC1 in the pellets of samples incubated with various concentrations of Ca^{2+}, suggesting that Ca^{2+} does not likely affect the binding of RIC1 to F-actin.

In addition, samples containing preformed F-actin, 1 μM RIC1, and various concentrations of Ca^{2+} were also subjected to low-speed centrifugation, and the resulting supernatants and pellets were analyzed by SDS-PAGE. As shown in Supplemental Figure 7H, although the amount of F-actin in the pellets was slightly reduced in the presence of 0.1, 1, and 10 μM Ca^{2+}, statistical analysis indicated that there was no significant difference between control reactions and reactions containing various concentrations of Ca^{2+} (Supplemental Figure 7H). To further investigate the effects of Ca^{2+} on RIC1-induced F-actin bundling in vitro, we observed samples of Alexa-488 phalloidin-labeled F-actin after incubation with both RIC1 and Ca^{2+} by spinning disc confocal microscopy. After incubation with RIC1 (0.5 μM) and Ca^{2+} (1 μM) for 30 min, F-actin was observed to form short bundles (Supplemental Figure 7D). These results confirm that the F-actin bundling activity of RIC1 is not notably altered in the presence of various concentrations of free Ca^{2+}. However, the presence of short F-actin bundles suggested that RIC1 might cause F-actin fragmentation in the presence of Ca^{2+}.

To further analyze the effect of RIC1 on F-actin fragmentation in the presence of free Ca^{2+}, we incubated various concentrations of RIC1 with preformed F-actin in the presence of 1.5 or 3 μM Ca^{2+} for 30 min. To measure the lengths of individual F-actin filaments, 100 mM NaCl was added to disperse the F-actin bundles after incubation. In the absence of RIC1 and Ca^{2+}, 100 mM NaCl did not affect the length of individual F-actin filaments (Supplemental Figures 8A, 8B, and 8I). In the presence of 1.5 μM RIC1 and 100 mM NaCl, the average length of individual F-actin filaments was not significantly different from the controls (with or without NaCl) (Supplemental Figures 8C and 8I). Incubation with 0, 0.6, 0.9, and 1.5 μM RIC1 in the presence of 3 μM Ca^{2+} and 100 mM NaCl resulted in average F-actin filament lengths of 14.8 ± 0.9, 11.3 ± 0.5, 7.8 ± 0.4, and 5.3 ± 0.3 μm, respectively (Supplemental Figures 8D to 8G and 8I). The average length of individual F-actin filaments was 8.3 ± 0.6 μm in the presence of 1.5 μM RIC1, 1.5 μM Ca^{2+}, and 100 mM NaCl (Supplemental Figures 8H and 8I). These results demonstrate that F-actin was fragmented in the presence of RIC1 and a micromolar range of free Ca^{2+} and that RIC1 fragmented F-actin in a dose-dependent manner. Collectively, these results indicate that RIC1 binds and fragments F-actin in the presence of a micromolar range of free Ca^{2+}.

We further analyzed whether RIC1 possessed F-actin severing activity by total internal reflection fluorescence microscopy (TIRFM). No notable breaks along individual rhodamine-labeled F-actin filaments were observed in the presence of RIC1 or Ca^{2+} alone (Figures 4D and 4E). However, after incubation with 100 μM Ca^{2+} and 0.05 μM RIC1, breaks were detected along F-actin filaments (Figure 4F; Supplemental Movie 4). The average severing frequencies in the presence of 0.05 μM RIC1 and various concentrations of free Ca^{2+} revealed a dependency on calcium. The number of breaks substantially increased with increasing

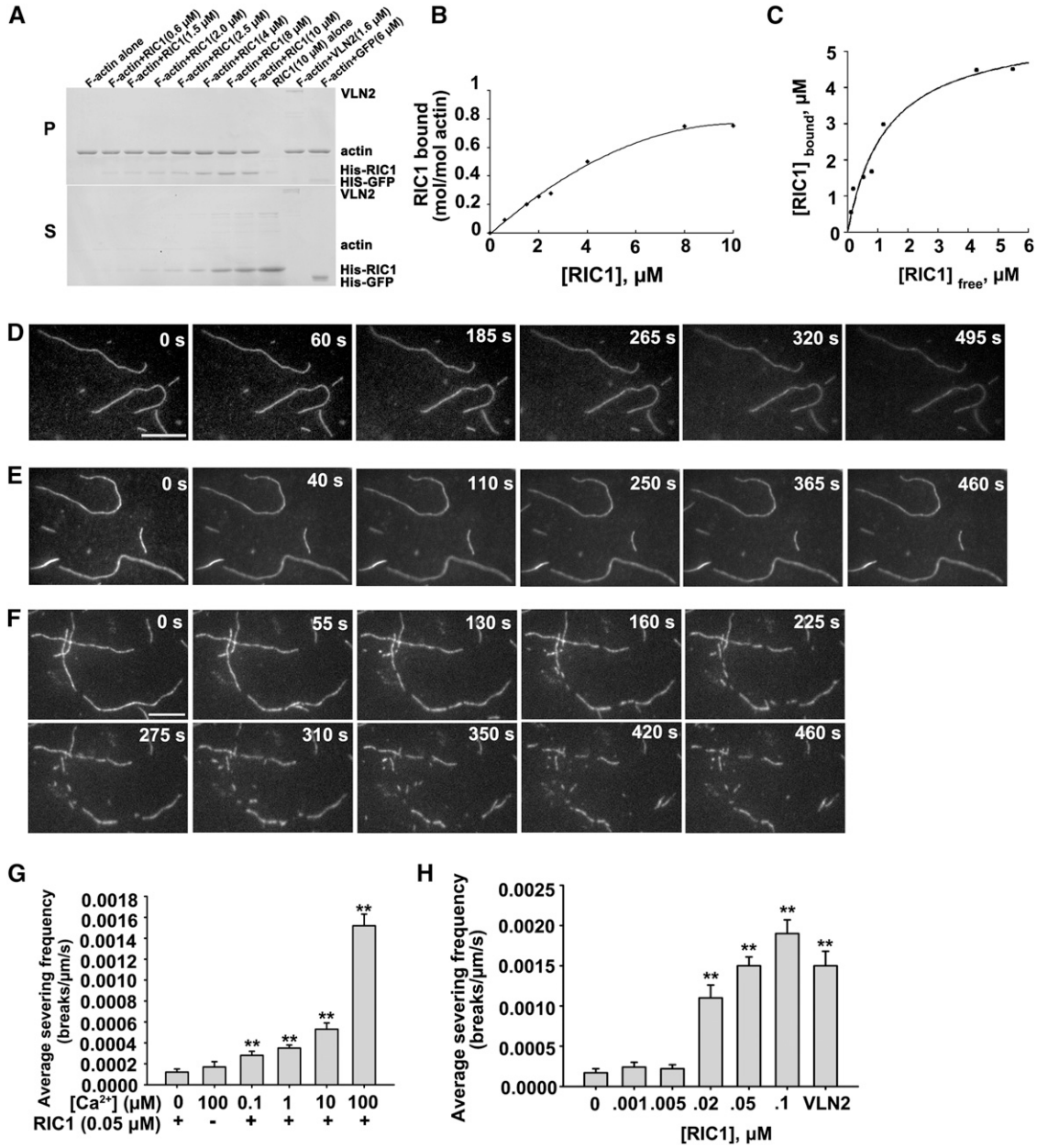

Figure 4. RIC1 Binds and Severs F-Actin in the Presence of Ca^{2+} in Vitro.

All data are presented as means ± SE. **P < 0.01, by Student's *t* test.

(A) A cosedimentation assay was performed to investigate whether RIC1 binds directly to F-actin. Various concentrations of recombinant RIC1 cosedimented with F-actin. Preformed F-actin was incubated with various concentrations of recombinant 6xHis-RIC1. VLN2 served as a positive control. RIC1 in the absence of F-actin and His-GFP served as negative controls. P, pellet; S, supernatant.

(B) Densitometry analysis of the results shown in **(A)**. Binding to F-actin was saturated at a stoichiometry of 0.75 mol RIC1/mol G-actin.

(C) The amount of RIC1 in the pellet (bound) was plotted versus the amount of RIC1 in the supernatant (free) and fitted with a hyperbolic function. The calculated K_d value was 0.76 μM for this representative experiment. The K_d from three experimental replicates was 0.74 ± 0.08 μM.

(D) and **(E)** Time-lapse images show that RIC1 has no effect on F-actin filament length in the absence of Ca^{2+}. F-actin (polymerized from 0.1 μM rhodamine-labeled G-actin) was incubated with either 100 μM Ca^{2+} **(D)** or 0.1 μM RIC1 **(E)**. No obvious changes in F-actin length were observed. Bar = 5 μm for **(D)** and **(E)**.

(F) Time-lapse images from Supplemental Movie 4. Preformed rhodamine-labeled F-actin was monitored by TIRFM immediately after the addition of 0.05 μM RIC1 and 100 μM Ca^{2+}. Individual F-actin filaments exhibited a notable increase in the number of breaks as time elapsed. Bar = 5 μm.

(G) F-actin severing frequencies (breaks·$\mu m^{-1}\cdot s^{-1}$) in the presence of 0.05 μM RIC1 and various concentrations of Ca^{2+} were measured (n = ~25 actin filaments per data set).

(H) Mean severing frequencies in the presence of various concentrations of RIC1 and 100 μM Ca^{2+} were plotted. Actin incubated in the presence of 0.002 μM VLN2 served as a positive control (n = ~25 actin filaments per experiment).

Ca^{2+} concentrations (Figure 4G). To quantify the F-actin severing activity of RIC1, we counted the breaks in the presence of 100 μM Ca^{2+} at various concentrations of RIC1 (Figure 4H). The average severing frequency increased sharply at levels of RIC1 > 0.02 μM (Figure 4H). These results demonstrate that RIC1 severs F-actin in a concentration-dependent manner. Therefore, we concluded that RIC1 severs F-actin in the presence of Ca^{2+} in vitro.

RIC1 Caps Actin Filaments in Vitro

We next sought to determine whether RIC1 associates with actin filaments after its severing. To determine this, prepolymerized short actin filaments were labeled with Alexa-488 phalloidin and used as seeds. Rhodamine-labeled actin was added to generate dual-color actin filaments with red barbed ends (Figures 5A to 5C). The resulting dual-color actin filaments were incubated with 2 μM His-RIC1 in the presence of 0.05 μM Ca^{2+} in vitro for 5 min. His-RIC1 was visualized by staining with anti-His antibody and a Dylight 405-conjugated secondary antibody. Actin filaments were severed into fragments by RIC1, and the RIC1 signal (blue dots) associated with one end of the actin fragments was also detected. Interestingly, those end-associated RIC1 blue dots were attached exclusively to the red barbed end of a dual-color filament (Figures 5B and 5C), which suggests a potential role of RIC1 at the barbed ends of actin filaments.

Next, we determined whether the presence of RIC1 altered the behavior of the ends of actin filaments. We initially performed a dilution-mediated actin depolymerization assay. Pyrene-labeled F-actin was diluted with G-buffer (containing 2 mM EGTA to chelate redundant free Ca^{2+}) containing various concentrations of RIC1, and F-actin fluorescence was monitored. As shown in Figure 5D, RIC1 reduced the rate of depolymerization in a dose-dependent manner. To test whether Ca^{2+} affected this process, various concentrations of free Ca^{2+} were added to F-actin in the presence of 0.12 μM RIC1. The resulting data revealed that the reduction in depolymerization was significantly enhanced with increases in Ca^{2+} concentration (Figure 5E). Given that RIC1 severs actin filaments in a calcium-dependent manner, treatment with RIC1 should fragment actin filaments to generate more free ends that would enhance depolymerization in the presence of Ca^{2+}. However, given that the opposite result was observed, we hypothesized that RIC1 may have a capping activity. Certainly, we cannot completely rule out the contribution of the filament side binding activity of RIC1 here.

To further test more directly whether RIC1 has capping activity, we performed a seeded actin elongation assay as described previously (Huang et al., 2005). In this elongation assay, profilin-bound actin is used to inhibit spontaneous nucleation and prevent monomer addition onto F-actin filaments at the pointed ends. However, profilin-bound actin can still be added to the barbed end to elongate F-actin. If the F-actin barbed end is capped by ABPs, the elongation of F-actin will be dramatically reduced. Preformed F-actin was diluted in G-buffer containing various concentrations of RIC1. G-actin (1 μM, with 10% pyrene-labeled actin), combined with human profilin I (3 μM), was then added to the preformed F-actin filaments to initiate actin filament elongation at the barbed ends. The elongation process was traced by monitoring the change in fluorescence. As shown in Figure 5F, RIC1 reduced the initial rate of elongation in a dose-dependent manner, and the K_d of RIC1 binding to the barbed ends of actin filaments was determined to be 1.8 μM. To test whether Ca^{2+} affected this process, we added various concentrations of free Ca^{2+} to the reaction in the presence of 0.8 μM RIC1. Results from these reactions demonstrated that increasing Ca^{2+} concentrations significantly enhanced the RIC1-induced reduction of elongation (Figure 5G). Therefore, we concluded that RIC1 caps F-actin at barbed ends to inhibit actin filament elongation and depolymerization at the barbed ends.

RIC1 Severs F-Actin at the Tip of Pollen Tubes

Because RIC1 localized to the apical PM of pollen tubes (as described above; Wu et al., 2001), we speculated that RIC1 most likely severs F-actin in the pollen tube tip region, where a high Ca^{2+} gradient exists. To assess this hypothesis, we captured time-lapse images of pollen tube tips at 2-s intervals (Figure 6A; Supplemental Movies 5 to 7). To quantify the severing capacity of RIC1, we measured two parameters (Staiger et al., 2009), the lifetime and maximum length of single F-actin filaments associated with the apical dome PM in wild-type Col-0, *ric1-1 (Col-0)*, and *OX 9* pollen tubes.

The distribution of measured lifetimes of single F-actin filaments is presented as the percentage of total F-actin filaments present in each of five bins (0 to 2, 2 to 6, 6 to 10, 10 to 14, and >14 s; Figure 6B). The lifetimes of apical PM-associated F-actin filaments were primarily distributed across three time ranges (0 to 2, 2 to 6, and 6 to 10 s; Figures 6A and 6B) in Col-0 pollen tubes. However, a greater percentage of PM-associated F-actin filaments had longer lifetimes in *ric1-1 (Col-0)* pollen tubes compared with wild-type tubes. Consistent with this observation, PM-associated F-actin was short-lived and largely distributed in the time range of 0 to 2 s (66.5% ± 7.3%) in *RIC1 OX 9* pollen tubes. These results indicate that the lifetime of PM-associated F-actin filaments was longer in *ric1-1 (Col-0)* pollen tubes and shorter in *OX 9* pollen tubes compared with wild-type pollen tubes.

We also measured the maximum length of single F-actin filaments associated with the apical and subapical PM in Col-0, *ric1-1 (Col-0)*, and *RIC1 OX 9* pollen tubes (n = ~80 actin filaments from 20 pollen tubes per line) (Figures 6A and 6C). These data indicate that the maximum length of single PM-associated F-actin filaments was longer in *ric1-1 (Col-0)* pollen tubes, but shorter in *RIC1 OX 9* pollen tubes, compared with wild-type pollen tubes.

The results suggest that the frequency of severing single actin filaments was decreased in *ric1-1 (Col-0)* pollen, resulting in a longer lifetime and maximum length of single F-actin filaments associated with the PM. By contrast, F-actin severing frequency was increased in *OX 9* pollen, leading to a shorter lifetime and decreased maximum length of PM-associated F-actin. The average severing frequency of PM-associated F-actin filaments in Col-0, *ric1-1 (Col-0)*, and *OX 9* pollen tubes confirmed this conclusion (Figure 6D).

PM Localization of RIC1 Is Important for Its Function

To further investigate whether the PM localization of RIC1 is important for RIC1 function, we monitored the distribution of

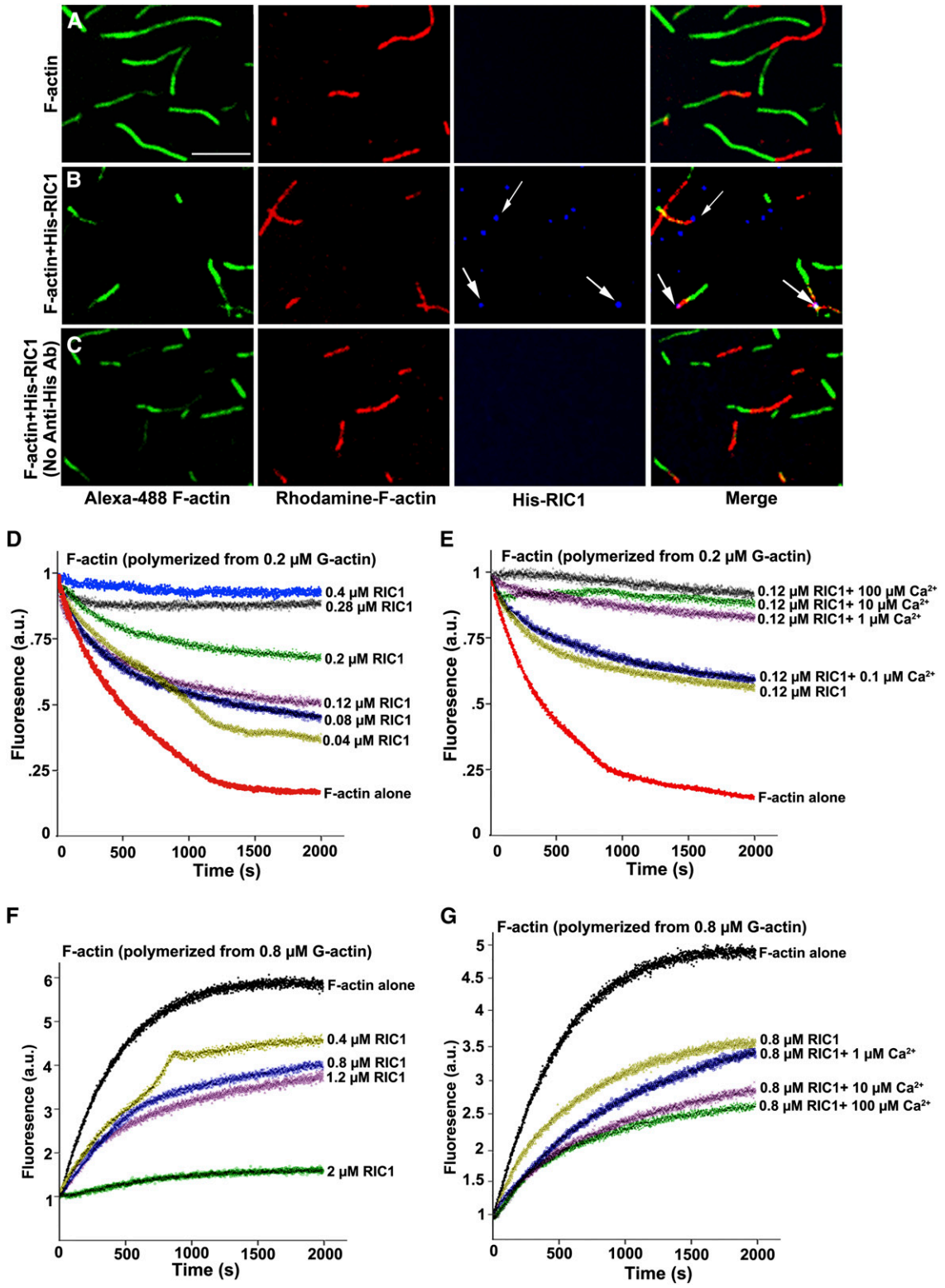

Figure 5. RIC1 Caps the Barbed Ends of F-Actin in Vitro.

(A) Dual-color actin filaments displaying polarity. Prepolymerized actin filaments were labeled with Alexa-488 phalloidin and used as seeds. Rhodamine-labeled actin was added to generate dual-color actin filaments with red barbed ends. Bar = 5 μm for **(A)** to **(C)**.

RIC1 at the PM in growing pollen tubes. The complemented line *COM 11*, which expresses RIC1-GFP, was used for analysis. The total amount of RIC1 at the apical PM was measured as described by Hwang et al. (2005). As shown in Figure 7A, the distribution of RIC1 was indicated by the fluorescence intensity of RIC1-GFP at the apical PM. The RIC1-GFP signal was highly dynamic at the tip PM (as shown in a representative growing pollen tube in Figure 7B, Supplemental Figure 9A, and Supplemental Movie 8). To further assess whether pollen tube growth is related to RIC1 localization, we treated pollen tubes with −20°C for 6 min to suspend growth and observed RIC1 localization. Although the RIC1-GFP signal was still detected at the tip PM in the absence of pollen tube growth, the oscillation was decreased. When pollen tube growth resumed, the oscillatory behavior was also recovered, and RIC1 oscillation was fully recovered prior to the full recovery of growth rate oscillation (Figure 7C; Supplemental Figure 9B and Supplemental Movie 9). These results suggest that the oscillation of RIC1 levels at the PM is related to pollen tube growth.

To test whether the localization of RIC1 at the PM is important for its effects on pollen tube growth, we expressed a mutated RIC1 protein containing two point mutations in the conserved residues His-37 and His-40, which lie within the CRIB motif, in pollen tubes. A previous study demonstrated that this mutant protein ($RIC1^{H37D/H40D}$) exhibits a dramatically reduced interaction with active ROP1 and loss of PM localization (Wu et al., 2001). Our observations after transient expression in tobacco (*Nicotiana tabacum*) pollen tubes confirmed that $RIC1^{H37D/H40D}$-GFP localizes to the cytoplasm but not the PM (Figure 8A). In comparison with control pollen tubes expressing only GFP, pollen tube elongation was dramatically reduced by RIC1 overexpression. Although transient overexpression of $RIC1^{H37D/H40D}$ also reduced pollen tube growth, its effect on pollen tube growth was much weaker (Figure 8B). Similar to tobacco, stably expressed $RIC1^{H37D/H40D}$-GFP was present only in the cytoplasm of Arabidopsis pollen tubes, whether it was expressed under the control of its native promoter or the Lat52 promoter (Figure 8C). We further investigated whether $RIC1^{H37D/H40D}$ affects pollen germination and pollen tube growth when stably overexpressed in *ric1-1* pollen (to minimize the influence of native wild-type RIC1). *ProLat52:GFP* and *ProLat52:RIC1-GFP* transgenic plants served as controls. As shown in Figure 8D, two transgenic lines with strong GFP signals for each transformation were used for further analysis. The fluorescence intensity in pollen grains was measured to indicate the expression levels of *RIC1* in these six transgenic lines (Figure 8E). In contrast with the overexpression of RIC1, $RIC1^{H37D/H40D}$ overexpression minimally affected pollen germination (Figure 8D). However, the average lengths of *ric1-1* pollen tubes overexpressing $RIC1^{H37D/H40D}$-GFP (lines 6 and 22) were shorter than those of *ric1-1* pollen tubes overexpressing GFP alone (lines 5 and 6). The reduction of pollen tube growth caused by the overexpression of $RIC1^{H37D/H40D}$-GFP was much weaker than that induced by RIC1-GFP overexpresssion (lines 1 and 11; Figures 8D and 8F). Because $RIC1^{H37D/H40D}$-GFP did not localize to the pollen tube PM, the dramatically reduced effects of this mutant form of RIC1 on pollen germination and pollen tube elongation demonstrated that the PM localization of RIC1 in the tip is important for the functioning of RIC1 in pollen tubes. Considering that $RIC1^{H37D/H40D}$-GFP overexpression still reduces pollen tube growth to a certain extent, we propose that RIC1 might also play a role in the cytoplasm to regulate pollen tube growth.

To test whether the H37D/H40D mutation affected the F-actin binding or bundling activities of RIC1, we purified the recombinant $RIC1^{H37D/H40D}$ protein. We then incubated Alexa-488 phalloidin-labeled F-actin with the mutant protein and observed the effects with a spinning disc confocal microscope. F-actin incubated in the absence of $RIC1^{H37D/H40D}$ and Ca^{2+} served as a control (Figure 8G). After incubation of preformed F-actin and 0.2 μM $RIC1^{H37D/H40D}$ for 30 min, F-actin was found to be organized into massive bundles (Figure 8H). $RIC1^{H37D/H40D}$ fragmented F-actin in the presence of 0.5 μM Ca^{2+} (Figure 8I). This result indicates that the mutation did not affect the F-actin bundling activity or the Ca^{2+}-dependent F-actin severing activity of RIC1 in vitro. Therefore, it is reasonable to predict that $RIC1^{H37D/H40D}$ could still sever F-actin in the cytoplasm of pollen tubes.

We investigated the effect of $RIC1^{H37D/H40D}$ on F-actin organization and dynamics in the apex of pollen tubes. Using rhodamine-phalloidin staining, we compared F-actin organization in *ProLat52:*

Figure 5. (continued).

(B) His-RIC1 (arrows) associated with the barbed ends of dual-color actin filaments. His-RIC1 was visualized by staining with anti-His antibody and a Dylight 405-conjugated secondary antibody.

(C) Similar associations were not observed in samples that were stained with secondary antibody alone.

(D) F-actin was diluted with G buffer in the presence of various concentrations of RIC1. RIC1 prevented actin depolymerization from the barbed ends in a dose-dependent manner. A single representative experiment ($n = 3$) is shown. a.u., arbitrary units.

(E) Preformed F-actin was diluted with G buffer containing 0.12 μM RIC1 in the presence of various concentrations of free Ca^{2+}. RIC1-induced reduction of F-actin depolymerization was significantly enhanced with increasing Ca^{2+} concentrations. The red trace shows the negative control in which F-actin was diluted with G buffer alone.

(F) and **(G)** Preformed F-actin seeds were incubated with various concentrations of RIC1 **(F)** or with 0.8 μM RIC1 in the presence of various concentrations of free Ca^{2+} **(G)**, and 1 μM 10% pyrene-labeled G-actin saturated with 3 μM human profilin I was added to initiate actin elongation at the barbed end. Polymerization was monitored by tracking the increase in pyrene-actin fluorescence upon assembly. A reaction without RIC1 and free Ca^{2+} served as a negative control (black traces). RIC1 reduced the initial rate of elongation in a dose-dependent manner, and increasing Ca^{2+} concentrations significantly enhanced the RIC1-induced reduction of F-actin elongation.

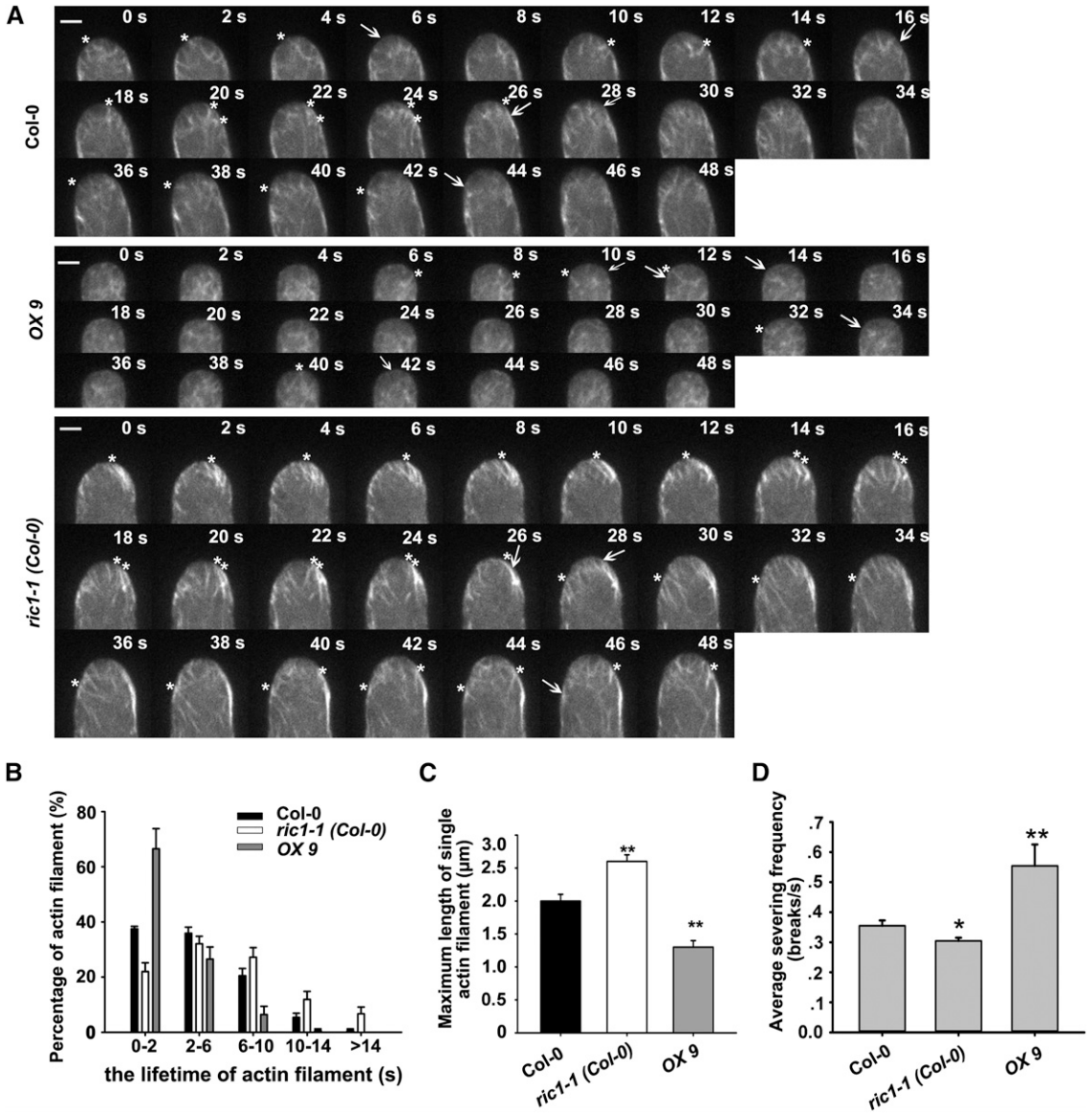

Figure 6. Quantitative Analysis of Apical/Subapical F-Actin in Pollen Tubes.

All data are presented as means ± SE. *P < 0.05, **P < 0.01, by Student's *t* test.

(A) F-actin dynamics were visualized by expressing Lifeact-mEGFP in Col-0, *OX 9*, and *ric1-1 (Col-0)* pollen tubes. Images were taken at 2-s intervals. Asterisks indicate individual F-actin filaments initiated from the PM. Arrows indicate F-actin severing events. Bars = 2 μm.

(B) The lifetimes of individual PM-associated F-actin filaments were analyzed in Col-0, *ric1-1 (Col-0)*, and *OX 9* pollen tubes. Approximately 80 actin filaments from 20 pollen tubes were monitored for each line. The distributions of the lifetimes are presented as the percentage of F-actin lifetimes falling within five ranges (0 to 2, 2 to 6, 6 to 10, 10 to 14, and >14 s). Filament lifetimes were longer in *ric1-1 (Col-0)* pollen tubes and shorter in *RIC1 OX 9* pollen tubes than in wild-type tubes.

(C) The average maximum length of single PM-associated F-actin filaments was analyzed in Col-0, *ric1-1 (Col-0)*, and *OX 9* pollen tubes. Approximately 80 actin filaments from 20 pollen tubes were monitored for each line. The maximum length reached by single F-actin filaments was longer in *ric1-1 (Col-0)* pollen tubes and shorter in *RIC1 OX 9* tubes compared with wild-type tubes.

(D) The average severing frequency of actin filaments was analyzed in Col-0, *ric1-1 (Col-0)*, and *OX 9* pollen tubes. The break of actin filaments from the PM was considered the severing event. Approximately 10 pollen tubes were monitored for each line.

RIC1-GFP (ric1-1)-1 and *ProLat52:RIC1*$^{H37D/H40D}$ *(ric1-1)-6* pollen tubes to control *ProLat52:GFP (ric1-1)-11* pollen tubes. Although the apical F-actin fluorescence intensity was significantly reduced in pollen tubes overexpressing RIC1$^{H37D/H40D}$, the reduction was less severe than the reduction in intensity caused by overexpressing wild-type RIC1 (Supplemental Figure 10). We transiently coexpressed RIC1 or RIC1$^{H37D/H40D}$ mutant proteins together with Lifeact-mEGFP in tobacco pollen tubes by particle bombardment to observe F-actin dynamics during pollen tube growth using spinning disc

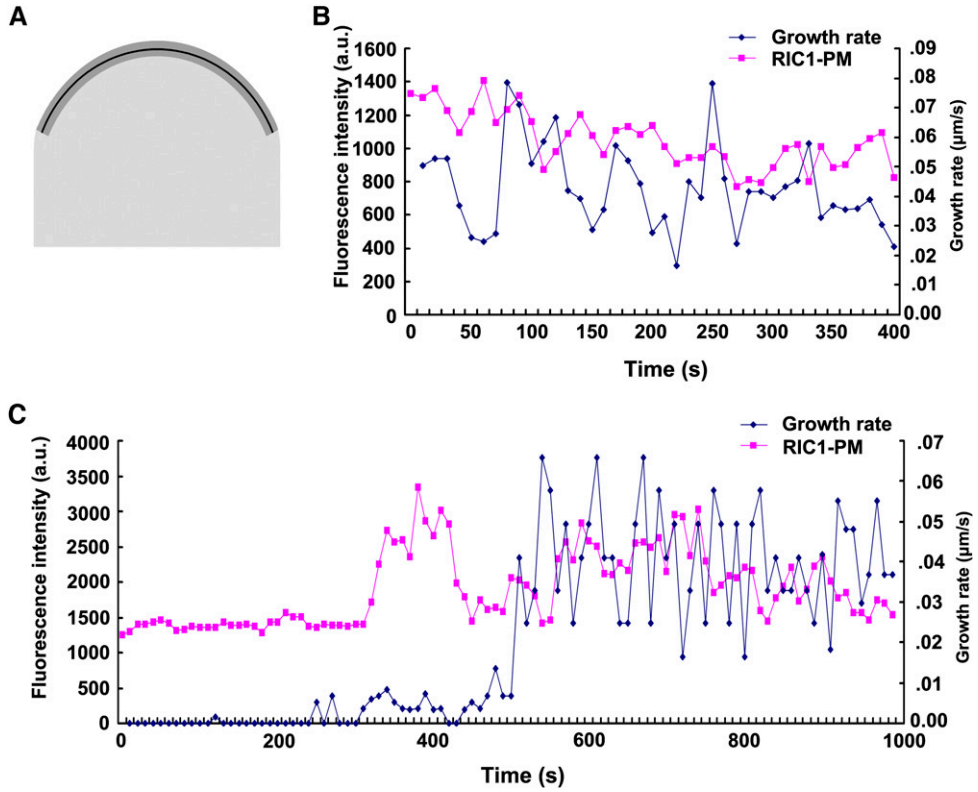

Figure 7. The Distribution of RIC1 at the PM Oscillates during Pollen Tube Growth.

A quantitative analysis of the localization of RIC1-GFP to the apical PM in growing pollen tubes is shown.
(A) Schematic illustrating how the amount of apical PM-localized RIC1-GFP was measured. A thin black line was superimposed on the PM. RIC1-GFP localization is represented by thick gray shading. The fluorescence intensity associated with the black line was measured to assess the amount of apical PM-localized RIC1-GFP.
(B) Oscillations in the growth rate and the intensity of PM-localized RIC1-GFP were measured in the growing tube shown in Supplemental Movie 8. a.u., arbitrary units.
(C) Oscillations in the growth rate and the intensity of PM-localized RIC1-GFP were measured in a tube that was treated with −20°C for 6 min and subsequently warmed to room temperature to resume growth (shown in Supplemental Movie 9). Recovery of RIC1-GFP oscillation precedes the recovery of growth rate oscillation.

confocal microscopy. Representative pollen tubes expressing various constructs are shown in Figures 9A and 9B. There were fewer apical F-actin structures in the pollen tube expressing RIC1$^{H37D/H40D}$ than in the control pollen tube expressing only Lifeact-mEGFP. However, apical F-actin structures in the pollen tube expressing wild-type RIC1 were the fewest. The average fluorescence intensity measurements reveal that overexpression of a mutant form of RIC1 without apical PM localization had a different impact on apical F-actin structures compared with wild-type RIC1 (Figure 9C), suggesting that the PM localization of RIC1 is important for its function on F-actin organization and dynamics during pollen tube growth.

DISCUSSION

We found that RIC1 can sever and cap F-actin in the presence of Ca^{2+} in vitro and that PM-localized RIC1 regulates pollen tube growth by manipulating the organization and dynamics of apical/subapical F-actin.

RIC1 Functions at the PM and in the Cytosol to Regulate Apical F-Actin Abundance and Dynamics

F-actin is continuously generated from the apical PM within the apical dome (Cheung and Wu, 2004; Cheung et al., 2010; Qu et al., 2013). Prompt and efficient disassociation of PM-nucleated filaments is critical for generating and maintaining the highly dynamic population of F-actin in the tip regions of pollen tubes. However, the mechanism that underlies the disassociation of PM-nucleated F-actin from the PM remains largely unknown. Evidence suggests that the F-actin severing activity of VLN2 and VLN5 facilitates the construction of actin collars/fringes under physiological calcium concentrations and that linear F-actin dissociates from the apical PM via severing in wild-type pollen tubes (Qu et al., 2013). However, no ABP has

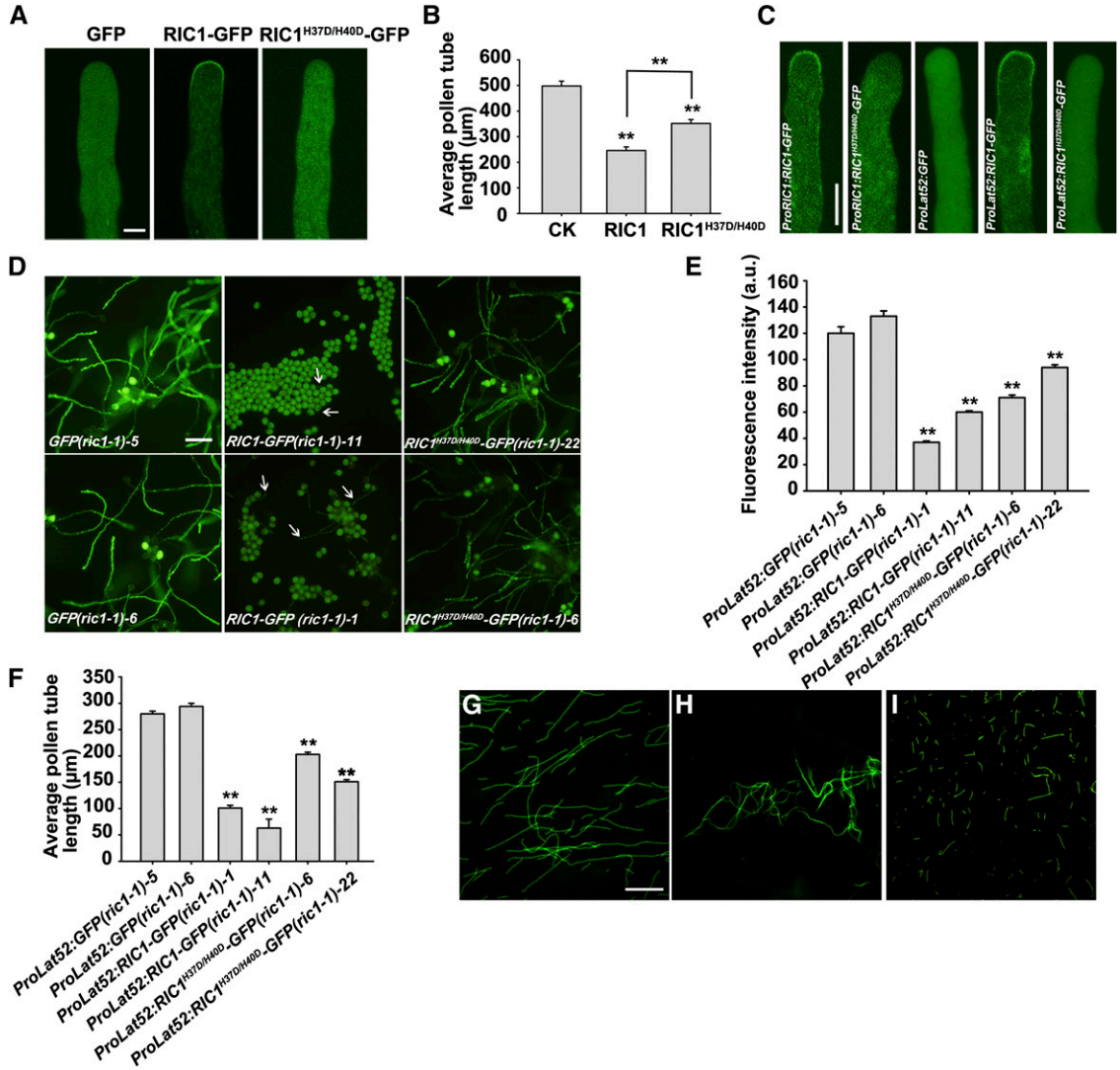

Figure 8. PM Localization of RIC1 Is Important for Its Function in Regulating Pollen Tube Growth.

All data are presented as means ± SE. *P < 0.05, **P < 0.01, by Student's *t* test.

(A) RIC1$^{H37D/H40D}$ contains two point mutations in conserved residues (His-37 and His-40) within the CRIB motif. GFP-tagged RIC1$^{H37D/H40D}$ localized exclusively to the cytoplasm in pollen tubes. Bar = 5 μm.

(B) *ProLat52:RIC1* or *ProLat52:RIC1$^{H37D/H40D}$* was transiently expressed with *ProLat52:GFP* in tobacco pollen tubes. Pollen tubes transiently expressing *ProLat52:GFP* served as controls. The average lengths of pollen tubes were measured 5 h after bombardment. Expression of RIC1 resulted in a dramatic reduction of pollen tube growth. Although the expression of RIC1$^{H37D/H40D}$ also reduced pollen tube growth, the degree of reduction was significantly less than that caused by RIC1-GFP. *n* > 90 pollen tubes per transformation. CK, control pollen tubes expressing *ProLat52:GFP* only.

(C) Localization of stably expressed RIC1-GFP and RIC1$^{H37D/H40D}$-GFP expressed under the control of the *RIC1* native promoter or the Lat52 promoter in Arabidopsis pollen tubes. RIC1-GFP localized to the apical PM under the control of both promoters. RIC1$^{H37D/H40D}$-GFP was present only in the cytoplasm. Arabidopsis pollen tubes stably expressing *ProLat52:GFP* served as a control. Bar = 5 μm.

(D) Constructs containing *GFP*, *RIC1-GFP*, and *RIC1$^{H37D/H40D}$-GFP* under the control of the Lat52 promoter were stably transformed into *ric1-1* plants. Overexpression of RIC1-GFP dramatically reduced pollen germination as well as pollen tube growth (pollen tubes indicated by arrows). Overexpression of RIC1$^{H37D/H40D}$-GFP minimally affected pollen germination. Bar = 100 μm.

(E) Quantification of the fluorescence intensity associated with pollen grains from *ProLat52:GFP (ric1-1)*, *ProLat52:RIC1-GFP (ric1-1)*, and *ProLat52:RIC1$^{H37D/H40D}$-GFP (ric1-1)* plants as shown in **(D)**. Although the fluorescence intensity in *ProLat52:RIC1-GFP (ric1-1)* pollen grains was much lower (indicating a lower relative expression level) than that of *ProLat52:GFP (ric1-1)* and *ProLat52:RIC1$^{H37D/H40D}$-GFP (ric1-1)* pollen, expression of *RIC1-GFP* resulted in greater inhibitory effects than expression of *RIC1$^{H37D/H40D}$-GFP* **(D)**. a.u., arbitrary units.

(F) Average lengths of pollen tubes from the transgenic lines shown in **(D)**. Overexpression of RIC1$^{H37D/H40D}$-GFP reduced pollen tube growth, but less severely than RIC1-GFP overexpression. *n* = ~300 pollen tubes per line.

(G) to **(I)** F-actin stained with Alexa-488 phalloidin was incubated alone **(G)**, with 0.2 μM RIC1$^{H37D/H40D}$ **(H)**, or with 0.2 μM RIC1$^{H37D/H40D}$ and 0.5 μM free Ca^{2+} **(I)**. The H37D/H40D point mutation did not affect the F-actin bundling and severing activity of RIC1. Bar in **(G)** = 5 μm for **(G)** to **(I)**.

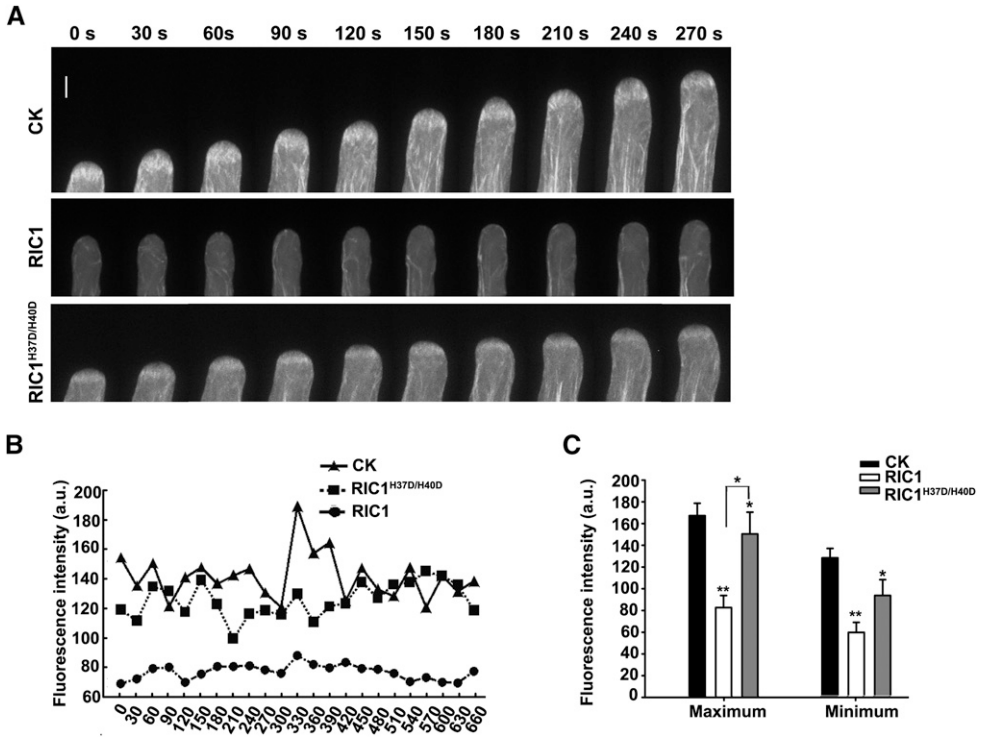

Figure 9. Different Impacts of RIC1$^{H37D/H40D}$ and RIC1 Overexpression on the Organization and Dynamics of Apical F-Actin.

All data are presented as means ± SE. *P < 0.05, **P < 0.01, by Student's *t* test.

(A) Time-lapse images were taken from tobacco pollen tubes 2 to 4 h after particle bombardment, showing F-actin dynamics in growing tobacco pollen tubes. CK, control pollen tubes transiently expressing *ProLat52:Lifeact-mEGFP* only. Bar = 5 μm.

(B) Oscillations in apical fine F-actin were quantified by measuring fluorescence intensity in growing tobacco pollen tubes, shown in **(A)**. a.u., arbitrary units.

(C) Average maximum and minimum fluorescence intensities of F-actin in the apical region of tobacco pollen tubes expressing *ProLat52:Lifeact-mEGFP* only (n = 13), *ProLat52:Lifeact-mEGFP* with *ProLat52:RIC1* (n = 11), or *ProLat52:Lifeact-mEGFP* with *ProLat52:RIC1$^{H37D/H40D}$* (n = 7). The decrease in fluorescence intensity caused by *RIC1$^{H37D/H40D}$* overexpression was less severe than the reduction in intensity due to overexpressing wild-type RIC1.

been reported to sever F-actin at the apical PM. This study reports that RIC1 binds to, severs, and caps F-actin in the presence of Ca^{2+} in vitro and localizes at the apical PM in vivo. Additionally, the severing frequency of F-actin in the apical dome was notably decreased in *ric1-1* pollen tubes but increased in *OX 9* pollen tubes compared with wild-type pollen tubes. Furthermore, overexpression of a RIC1 mutant protein (RIC1$^{H37D/H40D}$) that does not localize to the PM resulted in less severe growth inhibition phenotypes and reductions in apical F-actin compared with overexpression of wild-type RIC1, suggesting that membrane localization is important for RIC1 function. We propose that RIC1 is able to sever F-actin at the PM, providing a mechanism for F-actin release from the PM to control F-actin dynamics in the tip region. These results suggest that RIC1 may also have an important function in the cytoplasm, given that non-membrane-associated RIC1$^{H37D/H40D}$ reduced pollen tube growth. By transient overexpression of RIC1 in pollen tubes, we observed very few F-actin structures in pollen tube tips. However, when RIC1$^{H37D/H40D}$ was overexpressed, apical fine F-actin was still detected, although it was less abundant than in pollen tubes expressing only Lifeact-mEGFP. This observation suggests that cytosolic RIC1 is also important for the organization and dynamics of fine F-actin structures in pollen tube tips. A working model for the function of RIC1 in pollen tubes is shown in Figure 10. RIC1 localizes to the PM at the pollen tube tip and severs F-actin filaments arising from the PM to release the PM-anchored F-actin into the cytoplasm. In the apical cytoplasm, where high Ca^{2+} concentrations are present, cytoplasm-localized RIC1 can still sever F-actin. In addition, the barbed end capping activity of RIC1 prevents actin filaments from elongating further. This model suggests that RIC1 likely regulates the formation and dynamics of apical/subapical F-actin structures as well as the abundance of F-actin in the pollen tube tips. Kroeger et al. (2009) proposed that actin polymerization propagates from the existing subapical actin fringe array. Our study does not exclude this possibility, and RIC1 might also take action in the formation of the fringe by severing actin filaments in the cytosol as well, although only PM-initiated F-actin was emphasized in our schematic model for simplicity.

Direct visualization of the dynamics of individual actin filaments showed that they mainly grow out from the apical membrane (Qu et al., 2013), which is presumably mediated by formins (Cheung et al., 2010). Thus, it is suggested that the barbed end of PM-anchored actin filaments is directed toward the PM. The

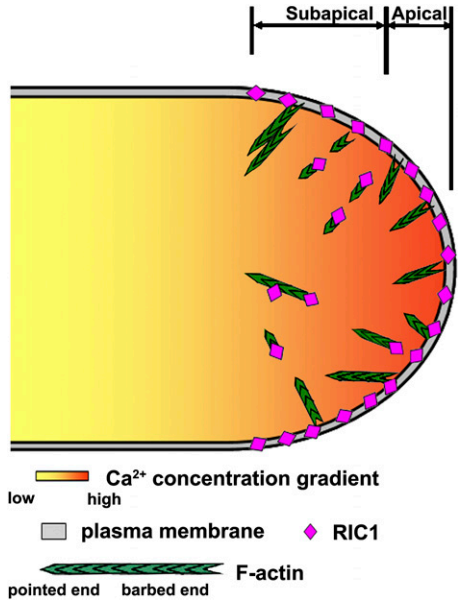

Figure 10. Working Model of RIC1-Mediated Regulation of F-Actin Dynamics in the Tips of Pollen Tubes.

Actin filament formation is initiated at the PM in the tip region of the pollen tube. PM-localized RIC1 severs F-actin from the PM, resulting in its dissociation, and facilitates rapid F-actin turnover in the pollen tube apex. The PM distribution of RIC1 oscillates during pollen tube growth, indicating that RIC1 moves between the PM and the cytoplasm. Cytoplasmic RIC1 is still capable of severing F-actin and, therefore, contributes to the formation and dynamics of apical/subapical F-actin structures in pollen tubes. RIC1 also caps the barbed ends of actin filaments to prevent elongation, further contributing to the regulation of the abundance of F-actin in the tip of the pollen tube.

apical PM localization of RIC1 suggests that RIC1 may interfere with the activity of formins by capping the barbed ends of actin filaments, besides releasing actin filaments via its severing activity. However, based on the estimated K_d of RIC1 binding to the barbed ends of actin filaments, the binding affinity was rather low compared with that of Arabidopsis CAPPING PROTEIN (Huang et al., 2003), At-FORMIN1(FH1-FH2) (Michelot et al., 2005), and At-FORMIN5 (Ingouff et al., 2005). Therefore, it is unlikely that RIC1 competes with formins to regulate actin dynamics via regulation of the behavior of the barbed ends of actin filaments.

In addition, oscillations in the distribution of RIC1 between the PM and the cytoplasm suggest that the functions of RIC1 in the PM and the cytoplasm must be coordinately regulated during pollen tube growth. This hypothesis will be a subject of our future investigations.

Actin Severing by Various Proteins May Contribute to Positive or Negative Control of Pollen Tube Elongation

In addition to RIC1, several actin regulators, such as VLN2, VLN5, MAP18, and MDP25, have been found to regulate pollen tube growth via actin filament severing activity in recent studies (Qu et al., 2013; Zhu et al., 2013; Qin et al., 2014). MAP18 is involved in regulating the growth direction of pollen tubes but has little effect on elongation rate. Although lack of or reduced VLN5, VLN2, MDP25, and RIC1 all caused increased actin filament length and lifetime, as well as decreased severing frequency in the tip of pollen tubes, the resulting pollen tube growth phenotypes varied. Growth inhibition in *vln2 vln5* pollen tubes suggests that VLN2 and VLN5 are positive regulators of pollen tube elongation, whereas the increased length of *mdp25* and *ric1* tubes indicates that MDP25 and RIC1 are negative regulators of pollen tube growth. A rational explanation is that the growth oscillation of pollen tubes is due to cooperation between positive and negative regulation of pollen tube elongation. This type of growth regulation requires the proper organization, abundance, and dynamics of apical/subapical F-actin structures that are coordinated by many ABPs, including various F-actin severing proteins that act at different sites and may affect the behavior of actin filaments in different ways. VLN2 and VLN5 are positive regulators of pollen tube elongation and have been found to be associated with actin filaments. They have also been demonstrated to promote actin turnover and facilitate the construction of actin collars/fringes (Qu et al., 2013). As a negative regulator of tube elongation, MDP25 is a PM-associated protein that is released from the PM in the apex (where high concentrations of Ca^{2+} exist) and destabilizes actin filaments in the cytosol at a subapical region of pollen tubes (Qin et al., 2014). Here, we report another negative regulator, RIC1, which regulates the abundance and oscillatory amplitude of fine F-actin in pollen tube tips, most likely by severing F-actin at both the apical PM and in the cytosol and capping the barbed ends of actin filaments. These F-actin severing proteins act together to regulate the proper organization, abundance, and dynamics of F-actin for normal pollen tube oscillatory growth.

The Distribution of RIC1 and Pollen Tube Growth

Pollen tubes grow in an oscillatory manner, which is regulated by a self-organizing signaling network involving a tip-localized ROP, tip-focused Ca^{2+} gradient, and interactions with the F-actin and vesicular trafficking pathways (Kost, 2008; Kroeger et al., 2008; Qin and Yang, 2011). This oscillatory manner of growth suggests that both positive and negative mechanisms regulate pollen tube growth. The observations presented in this study suggest that RIC1 negatively regulates pollen tube growth through the regulation of F-actin. Interestingly, the distribution of RIC1 at the tip PM of the pollen tube oscillates during pollen tube growth. When pollen tube growth was arrested by low-temperature treatment, RIC1 remained localized to the PM, but its oscillations ceased. When pollen tube growth resumed after transfer back to room temperature, the oscillation of PM-distributed RIC1 resumed as well, and the full recovery of RIC1 oscillations preceded the full recovery of pollen tube growth oscillations. These observations suggest that the oscillatory behavior of RIC1 at the PM is related to the oscillations of pollen tube growth.

On the other hand, our experimental results also demonstrate that although $RIC1^{H37D/H40D}$ did not localize to the PM, overexpression of this protein altered apical F-actin organization and reduced pollen tube elongation, although less severely than overexpression of wild-type RIC1. Importantly, in vitro experiments

demonstrated that RIC1$^{H37D/H40D}$ retains the ability to bind and sever F-actin in the presence of Ca^{2+}. This observation suggests that non-membrane-localized RIC1 is still able to negatively regulate pollen tube growth in the cytoplasm. Therefore, RIC1 may negatively regulate pollen tube growth via its oscillating distribution between the PM and the cytoplasm, and it is likely that these oscillations are coordinated with or regulated by other positive regulators of pollen tube growth, such as Ca^{2+} and ROPs.

RIC1 belongs to the RIC protein family and is known as an effector of active ROPs (Wu et al., 2001). Three closely related ROPs, ROP1, ROP3, and ROP5, are expressed in Arabidopsis pollen (Li et al., 1998). ROP1 regulates pollen tube tip growth by manipulating apical F-actin dynamics through two counteracting downstream pathways involving RIC3-Ca^{2+}-mediated F-actin disassembly and RIC4-mediated F-actin assembly (Fu et al., 2001; Gu et al., 2005). However, neither RIC3 nor RIC4 interacts directly with F-actin. We predict that RIC1 is an effector that interacts directly with F-actin in ROP signaling pathways to precisely regulate apical F-actin. A mutation in the CRIB domain of RIC1 that inhibits interactions with active ROPs (Wu et al., 2001) abolished the apical PM localization of RIC1 and compromised its effects on pollen tube growth in an overexpression model, suggesting that RIC1-mediated modulation of apical F-actin in the pollen tube is also regulated by ROPs. Currently, we do not know the identity of the precise ROP that lies upstream of RIC1, but this study suggests that RIC1 regulates apical F-actin in concert with both Ca^{2+} signaling and ROP signaling. How does the oscillation of RIC1 regulate pollen tube growth oscillation? How do ROPs regulate the oscillation of RIC1 distribution between the PM and cytoplasm? Will multiple ROPs coordinately or counteractively regulate RIC1 in pollen tubes? These are interesting questions that remain to be answered.

Potential Mechanisms That Regulate RIC1 Activity on Cytoskeletal Elements

Previous reports, and this study, have identified various interactions between RIC1 and microtubules or F-actin in different types of cells or organs (Fu et al., 2005, 2009). These observations raise an interesting question regarding how the activities of RIC1 on different cytoskeletal elements are controlled or regulated in different cells and/or different cellular processes. As discussed above, RIC1 is a downstream effector of ROP GTPases. Binding of RIC1 to microtubules has been shown to require active ROP6, whereas ROP2 inhibits RIC1 activity on microtubules by recruiting it to the PM (Fu et al., 2005, 2009). Therefore, different ROPs may specifically regulate the activity of RIC1 on either microtubules or F-actin, although it remains unclear which ROP regulates RIC1 oscillations and activities on F-actin in pollen tubes. We have just started to investigate which ROP regulates RIC1's activity and how. We investigated whether ROP1 activity influenced the ability of RIC1 to bind, bundle, or sever actin filaments in vitro. A high-speed cosedimentation assay demonstrated that CA-rop1 had little effect on RIC1 binding to F-actin, whereas DN-rop1 compromised binding (Supplemental Figures 11A and 11B). However, a low-speed cosedimentation assay showed that both CA-rop1 and DN-rop1 reduced RIC1 bundling activity, although DN-rop1 had a stronger effect (Supplemental Figures 11C and 11D). In terms of RIC1 F-actin severing activity in the presence of Ca^{2+}, the addition of CA-rop1 did not affect the activity, but DN-rop1 inhibited RIC1 severing of F-actin (Supplemental Figures 11E to 11K). These data suggest an important role of ROP1 and perhaps other ROPs in the regulation of RIC1 functioning on F-actin dynamics during pollen tube tip growth. However, the precise mechanism underlying this activity will require further investigation.

Based on previous reports and this study, calcium is also a potential regulator. Here, we demonstrated that RIC1 exhibits Ca^{2+}-dependent F-actin severing activity in vitro. Furthermore, we found that RIC1-mediated severing and capping of F-actin at the apical PM and in the cytosol of pollen tubes are involved in the regulation of apical F-actin dynamics and pollen tube growth. Some other proteins that act on both microtubules and F-actin have been reported to have Ca^{2+}-dependent F-actin severing activity. For example, MAP18, which binds both microtubules and F-actin, severs F-actin in a Ca^{2+}-dependent manner (Zhu et al., 2013). A previous report based on pharmacological analysis suggested that an auxin-activated ROP6-RIC1 pathway inhibited PIN2 internalization by stabilizing F-actin in root cells (Lin et al., 2012). One possible explanation for these varying observations is that the Ca^{2+} concentrations present in the pollen tube tip differ from those in root cells (Monshausen et al., 2009). However, the precise manner by which the ROP6-RIC1 pathway acts to stabilize F-actin in root cells requires further study.

METHODS

Plant Material and Growth

The *Arabidopsis thaliana* Ws-2 and Col-0 ecotypes served as wild-type plants in this study. The *ric1-1* line (in the Ws-2 background) was obtained as described previously (Fu et al., 2005; Lin et al., 2012).

An Arabidopsis line expressing *ProLat52:Lifeact-mEGFP* was crossed to *ric1-1* and *RIC1 OX* transgenic plants to visualize F-actin in living pollen tubes. Arabidopsis seeds were germinated and grown on half-strength Murashige and Skoog medium supplemented with 1% sucrose and 0.8% agar for 7 d before transfer to soil. The seedlings were then incubated in a growth chamber under 16-h-light/8-h-dark conditions at 22°C. Tobacco (*Nicotiana tabacum*) plants were grown in a greenhouse at 28°C.

Plasmid Construction and Plant Transformation

A 2-kb region of the *RIC1* promoter was amplified from genomic DNA using the primers 5′-CTCGTGAAATCTGACATTGGTGG-3′ and 5′-TGGTCTATAAAGGGTTGGTTCCG-3′. The *RIC1* coding sequence was amplified using the primers 5′-TCTAGAATGGCGACGACAATGAAGG-3′ and 5′-GGTACCTCAGATAATATCGTTACAGGTTG-3′. The resulting DNA was subcloned into the pCAMBIA1300 vector under the control of the Lat52 promoter. The construct was introduced into Col-0 plants via *Agrobacterium tumefaciens*-mediated transformation (Clough and Bent, 1998). Five lines stably overexpressing *RIC1* were obtained, and two of these lines (named *RIC1 OX 9* and *RIC1 OX 15*) were used for further analyses.

RT-PCR/qRT-PCR Analysis

Total RNA from open flowers or pollen grains was extracted using TRIzol reagent (Invitrogen) according to the manufacturer's instructions. *RIC1* expression was analyzed via two-step RT-PCR and/or fluorescence

qRT-PCR using SYBR Green mix. To amplify the full-length coding region of *RIC1*, the forward primer 5′-ATGGCGACGACAATGAAGG-3′ and the reverse primer 5′-GATAATATCGTTACAGGTTGTATCA-3′ were used. *EF1αA4* (*EF1*) was amplified as an internal control using primers 5′-ATGCCCCAGGACATCGTGA-3′ and 5′-CGGCACCCTTAGCTGGATC-3′. For qRT-PCR, the primers used for *RIC1* were 5′-CCGACGGTCCAAC-CAACAC-3′ and 5′-GAGACCCGTTATGATTTGGAGAAG-3′. *18S* was amplified as an internal control using the primers 5′-CGGCTACCA-CATCCAAGGAA-3′ and 5′-TGTCACTACCTCCCCGTGTCA-3′.

GUS Staining

The native *RIC1* promoter (2 kb upstream of the ATG) was fused with a GUS reporter and cloned into the pCAMBIA1391 vector. The resulting construct was then transformed into Col-0 plants. T3 homozygous plants from five independent lines were used for histochemical staining of GUS activity. GUS staining was performed as described previously (Wang et al., 2007). Images were obtained using an Olympus microscope (SZX16 or BX51) equipped with a color CCD camera (DP72 or DP70).

Ballistics-Mediated Transient Expression in Tobacco Pollen Tubes

Freshly collected mature pollen grains were subjected to a particle bombardment procedure (Fu et al., 2001) to induce transient expression of RIC1. To visualize the subcellular localization of wild-type or mutant RIC1 in tobacco pollen tubes, the *RIC1* and *RIC1*$^{H37D/H40D}$ coding sequences (Wu et al., 2001) were fused with GFP at the C terminus and placed under the control of the *Lat52* promoter in the pUC19 vector. A mass of 0.5 μg of *ProLat52:RIC1-GFP* or *ProLat52:RIC1*$^{H37D/H40D}$*-GFP* plasmid was used for each bombardment (PDS-1000/He; Bio-Rad). Transformed pollen grains were incubated in pollen germination medium (10 μM $CaCl_2$, 1 mM KCl, 1 mM $MgSO_4$, 0.01% H_3BO_3, and 10% sucrose, pH 7.0) for 3 h prior to observation with a Zeiss confocal laser microscope (LSM META 510). To assess the effect of RIC1 expression on pollen tube growth, 0.5 μg of *ProLat52:RIC1* or *ProLat52:RIC1*$^{H37D/H40D}$, together with 0.5 μg of *ProLat52:GFP*, were used for bombardment. The pollen tubes were then observed with an Olympus fluorescence microscope (BX51) equipped with a CCD camera after 5 h of incubation in pollen germination medium. To investigate the effect of RIC1 on F-actin dynamics, 0.5 μg of *ProLat52:RIC1* or *ProLat52:RIC1*$^{H37D/H40D}$, together with 0.5 μg of *ProLat52:Lifeact-mEGFP*, were used.

Analysis of Pollen Tube Germination and Growth Rate in Vitro

Mature Arabidopsis pollen grains were collected and germinated on solid germination medium containing 5 mM $CaCl_2$, 5 mM KCl, 1 mM $MgSO_4$, 0.01% H_3BO_3, 10% sucrose, and 1.5% low-melting agarose (Invitrogen), pH 7.5 (adjusted with 0.1 M NaOH) (Boavida and McCormick, 2007). An Olympus microscope (BX51) equipped with a CCD camera was used to observe in vitro-germinated pollen tubes. The germination rate was determined after 1 or 1.5 h of incubation. A pollen grain was classified as germinated if the pollen tube length was equal to or greater than the pollen grain diameter, as described by Boavida and McCormick (2007). The pollen tube length was measured at 3 h after germination using ImageJ software.

To determine the growth rates of pollen tubes, images of each pollen tube were taken at two time points at a 5-min interval. To investigate the effect of LatB or oryzalin on pollen tube growth, various concentrations of the drugs were added to the germination medium.

Analysis of Pollen Tube Germination in Vivo

To observe in vivo-germinated pollen tubes in pistils, pollen and pollen tubes were stained with aniline blue as described by Schiott et al. (2004). Preemasculated mature wild-type flowers were pollinated with wild-type, *RIC1 OX*, or *ric1-1* pollen. The pollinated pistils were collected at 2, 4, 6, or 12 h after pollination and fixed in 10% acetic acid, 30% chloroform, and 60% ethanol, followed by incubation in 4 M NaOH overnight. The pistils were then stained for 8 h with 0.05% aniline blue in 50 mM potassium phosphate (pH 7.5) and pressed gently between a slide and a cover slip. Images were captured using an Olympus fluorescence microscope (BX51) equipped with a 10× objective and UV light excitation.

Immunofluorescence Microscopy of Microtubules in Pollen Tubes

To visualize the microtubule cytoskeleton in pollen tubes, we performed an indirect immunofluorescence staining assay on Arabidopsis pollen tubes as described in previous studies (Hwang et al., 2008; Cai et al., 2011) with minor modifications. Briefly, Arabidopsis pollen grains were germinated for 3 h on germination medium and later fixed for 1.5 h in 4% formaldehyde freshly prepared from paraformaldehyde containing 50 mM PIPES, pH 7.9, 2 mM EGTA, 2 mM $MgCl_2$, and 10% sucrose. After washing with PBS three times, the pollen tubes were digested with 1% cellulase (Sigma-Aldrich) and 0.1% pectolyase Y-23 (Yakult) in PBS at room temperature for 5 to 10 min. The resulting pollen tubes with digested cell walls were then washed with 0.1% Nonidet P-40 in PBS for 10 min, followed by two additional washes with 0.05% Nonidet P-40 in PBS. After washing, the pollen tubes were incubated in blocking buffer (50 mM glycin in PBS) at room temperature for 30 min. They were next incubated overnight with the primary antibody (mouse anti-α-tubulin) diluted 1:500 in PBS containing 0.05% Nonidet P-40. After three washes with 0.05% Nonidet P-40 in PBS, the pollen tubes were incubated at room temperature for 2 h with the secondary antibody (fluorescein isothiocyanate-conjugated goat anti-mouse IgG) diluted 1:500 in PBS containing 0.05% Nonidet P-40. After two washes with PBS, the microtubules were observed with a spinning disc confocal microscope (Yokogawa) using an Olympus IX81 microscope with a 100×/1.45 oil objective.

Rhodamine-Phalloidin Staining for Visualizing F-Actin in Pollen Tubes

Arabidopsis pollen tubes were incubated on germination medium for 3 h and then were fixed for 1 h in 350 μM MBS (Sigma-Aldrich; prepared in germination medium). The treated pollen tubes were washed with 0.1% Nonidet P-40 in germination medium for 10 min, followed by three additional washes (10 min each) with 0.05% Nonidet P-40 in TBSS buffer (50 mM Tris-HCl, 200 mM NaCl, and 10% sucrose, pH 7.5). Then, the pollen tubes were stained with 132 nM rhodamine-phalloidin (Sigma-Aldrich) in TBSS with 0.05% Nonidet P-40 at room temperature for 2 h. After two washes with TBSS, the stained pollen tubes were observed with a spinning disc confocal microscope using a 100×/1.45 oil objective.

Live-Cell Imaging

All fluorescent images of live pollen tubes were recorded with a spinning disc confocal microscope system (Yokogawa) using an Olympus IX81 microscope equipped with an Andor iXon CCD camera unless otherwise indicated. GFP was excited with a 488-nm argon laser, and emissions were collected through 525- ± 5.5-nm filters.

To visualize F-actin, pollen tubes expressing *ProLat52:Lifeact-mEGFP* were incubated on germination medium for 2 to 4 h and observed using a spinning disc confocal microscope with a 100×/1.45 oil objective. Z-stack images were captured with a 0.5-μm step size using a 150-ms exposure time. Time-lapse Z-stack images (0.5-μm step size) were captured over a 540-s time period at 30-s intervals with a 200-ms exposure time. To investigate F-actin severing events, time-lapse images were taken over a 48-s time period at 2-s intervals using a 150-ms exposure time, with a Z-series of two continued focal planes in the middle of a tube (0.5-μm step size) taken at each time point.

The subcellular localization of RIC1 in Arabidopsis pollen grains and tubes was analyzed by stably expressing *RIC1-GFP* under the control of its native promoter in *ric1-1* plants. Pollen grains and tubes germinated in vitro were observed under a spinning disc confocal microscope equipped with a 40× oil objective.

To investigate the dynamics of RIC1 localization in growing pollen tubes, pollen tubes expressing RIC1-GFP were incubated on solid germination medium for 3 h. A piece of solid medium with pollen tubes had been cut and transferred to a piece of cover glass before it was put in a −20°C refrigerator for 6 min. Then, the cover glass with pollen tubes was transferred to room temperature and was covered with another piece of cover glass for observation by spinning disc confocal microscopy using a 100×/1.45 oil objective. Time-lapse Z-stack images (0.5-μm step size) of the pollen tube apex were captured over a 990-s time period at 10-s intervals. Control pollen tubes (unfrozen tubes) were monitored for 400 s. The exposure time was 200 ms. The localization dynamics of RIC1 at the apical PM were quantified by measuring the fluorescence intensity using ImageJ.

To analyze F-actin dynamics in tobacco pollen tubes, pollen tubes transiently expressing *Lat52:Lifeact-mEGFP* were observed with a spinning disc confocal microscope using a 100×/1.45 oil objective 2 to 4 h after bombardment. Time-lapse Z-stack images (0.5-μm step size) were captured over a 270-s time period at 30-s intervals with a 200-ms exposure time.

FM4-64 Staining and Plasmolysis Assays

FM4-64 staining and plasmolysis assays were used to demonstrate that RIC1 is localized to the apical PM of pollen tubes. Loading *COM 11* pollen tubes with FM4-64 dye was generally achieved by the direct addition of 10 μM FM4-64 in the liquid medium. To achieve plasmolysis, liquid germination medium containing 25% mannitol was added to *COM 11* pollen tubes for 10 min before observation using spinning disc confocal microscopy.

Quantification of F-Actin Dynamics in Pollen Tubes

To quantify F-actin dynamics in pollen tubes, the F-actin fluorescence intensity at the pollen tube apex was measured using ImageJ. A semi-elliptical segment (distance = 2 μm) at the center of the extreme tip was selected for apical F-actin analysis. The corrected average fluorescent pixel intensity was assessed to estimate the relative amount of F-actin. The maximum or minimum fluorescence intensity was used to estimate the maximum or minimum relative amount of F-actin over a given period.

To quantify F-actin bundling at the shank and tip of pollen tubes, an average skewness value and F-actin density were measured using ImageJ as described previously (Higaki et al., 2010; Li et al., 2012).

To analyze the F-actin severing activity of RIC1 in the tip of pollen tubes, severing frequency, filament lifetime, and maximum length were measured as described previously (Staiger et al., 2009). Newly formed F-actin filaments arising from the PM were tracked and analyzed. The lifetime results were grouped into five bins: 0 to 2 s (including 2 s), 2 to 6 s, 6 to 10 s, 10 to 14 s, and >14 s. The maximum length a single F-actin filament reached prior to dissociation from the PM was also measured. ImageJ software was employed to analyze the data.

Colocalization of RIC1 with Polarity-Labeled Actin Filaments in Vitro

G-actin, rhodamine-labeled G-actin, and His-RIC1 were centrifuged at 200,000*g* for 1 h prior to use. Preformed F-actin (polymerized from 5 μM G-actin) was labeled with 5 μM Alexa-488 phalloidin (Sigma-Aldrich) and used as F-actin seeds. Rhodamine-labeled G-actin (5 μM) was then added and incubated for another 6 min. The resulting dual-color actin filaments displayed clear polarity with a red barbed end. The dual-color F-actin was diluted 50-fold and added to a flow cell coated with myosin and incubated for 5 min. Then, 2 μM His-RIC1 protein and 0.05 μM Ca^{2+} were applied to each flow cell. After a 5-min incubation with His-RIC1, samples were stained with an anti-His antibody (1:1000; Sigma-Aldrich) and a Dylight 405 goat anti-mouse IgG secondary antibody (1:100; Abbkine). Samples without RIC1 or stained with secondary antibody alone were used as negative controls. A spinning disc confocal system (Yokogawa) equipped with an Olympus IX81 microscope and an Andor iXon CCD camera was used to record the results. Alexa-488 was excited with a 488-nm argon laser; rhodamine was excited with a 561-nm laser; and Dylight 405 was excited with a 405-nm laser.

Cosedimentation Assays

The full-length *RIC1* coding sequence was cloned into the pET-30a vector, and 6xHis-RIC1 was expressed in *Escherichia coli* BL21 (DE3) cells. Purified 6xHis-RIC1 and G-actin were centrifuged at 200,000*g* for 30 min at 4°C prior to use. Actin was polymerized at 25°C for 30 min in 10× KMEI buffer (500 mM KCl, 10 mM $MgCl_2$, 10 mM EGTA, and 100 mM imidazole-HCl, pH 7.0). For high-speed cosedimentation assays, F-actin (polymerized from 6 μM G-actin) was incubated with various concentrations of 6xHis-RIC1 (0, 0.6, 1.5, 2.0, 2.5, 4, 8, and 10 μM) at room temperature for 30 min. After centrifugation at 100,000*g* for 15 min at 25°C, the resulting supernatant and pellet were separated. The pellets and supernatants were combined with loading buffer (250 mM Tris-HCl, 8% SDS, 20% glycerol, and 0.4% bromophenol blue) and then analyzed by SDS-PAGE using 10% acrylamide gels. The quantity and binding ratio of RIC1 and actin were measured using ImageJ software. The equilibrium K_d value was determined as described by Wu et al. (2010). RIC1 in the pellet ($[RIC1]_{bound}$) was plotted as a function of RIC1 in the supernatant ($[RIC1]_{free}$), and the data were fitted with a hyperbolic function using Kaleidagraph version 4.0 software (Synergy Software).

To determine whether Ca^{2+} affected the binding of RIC1 to F-actin, preformed F-actin (polymerized from 6 μM G-actin) and 6xHis-RIC1 (2.5 μM) were incubated in the presence of various concentrations of Ca^{2+} (0, 0.1, 1, 10, and 100 μM) for 30 min and were then subjected to high-speed centrifugation. The resulting supernatants and pellets were analyzed by SDS-PAGE using 10% acrylamide gels. The quantity and binding ratio of RIC1 and actin were measured using ImageJ software.

To test whether RIC1 affects the binding of Lifeact-GFP to F-actin, F-actin (polymerized from 6 μM G-actin) was combined with various concentrations of His-RIC1 (0, 6, and 10 μM) and Lifeact-GFP (5 and 15 μM) and incubated for 30 min at room temperature. After centrifugation at 50,000*g* for 15 min at 25°C, the resulting supernatant and pellet were separated. The pellets and supernatants were resuspended with loading buffer and analyzed by SDS-PAGE using 10% acrylamide gels.

To test whether CA-rop1(G15V) or DN-rop1(T20N) affects the binding of RIC1 to F-actin, F-actin (polymerized from 6 μM G-actin) was combined with various concentrations of His-RIC1 (2 and 4 μM) and CA- or DN-rop1 (1.5 and 3 μM) for 30 min at room temperature. After centrifugation at 50,000*g* for 15 min at 25°C, the resulting supernatant and pellet were separated. The pellets and supernatants were resuspended with loading buffer and analyzed by SDS-PAGE using 10% acrylamide gels.

For low-speed cosedimentation assays, F-actin (polymerized from 8 μM G-actin) was incubated with various concentrations of 6xHis-RIC1 (0, 0.1, 0.2, 0.4, 0.6, 1.0, and 1.6 μM) at room temperature for 30 min. After centrifugation at 3000*g* for 30 min at 25°C, the resulting supernatants and pellets were separated. The pellets and supernatants were then combined with loading buffer and analyzed by SDS-PAGE using 10% acrylamide gels. The quantity and rate of F-actin bundle formation were measured using ImageJ software. To assess whether Ca^{2+} affected the F-actin-bundling activity of RIC1, preformed F-actin (polymerized from 8 μM G-actin) and 1 μM 6xHis-RIC1 were incubated with various concentrations of Ca^{2+} (0, 0.01, 0.1, 1, 10, and 100 μM) for 30 min and then subjected to low-speed centrifugation. The resulting supernatants and

pellets were analyzed by SDS-PAGE, and the quantity and rate of F-actin bundle formation were measured using ImageJ software.

To test whether CA-rop1 or DN-rop1 affected the F-actin bundling activity of RIC1, F-actin (polymerized from 6 μM G-actin) was incubated with various concentrations of His-RIC1 (2 μM) and rop1s (1.5 and 3 μM) or His-RIC1 (4 μM) and rop1s (1.5 and 3 μM) for 30 min at room temperature. After centrifugation at 3000*g* for 30 min at 25°C, the resulting supernatants and pellets were separated. The pellets and supernatants were resuspended with loading buffer and analyzed by SDS-PAGE using 10% acrylamide gels.

Visualization of F-Actin Organization and Dynamics in Vitro

G-actin and other proteins were centrifuged at 100,000*g* for 30 min prior to use. For visualization of F-actin bundling, F-actin (polymerized from 0.5 μM G-actin) was incubated with or without 1 μM Ca^{2+} in the presence of 0.5 μM RIC1 for 30 min at room temperature. The F-actin was then stained with 0.5 μM Alexa-488 phalloidin (Sigma-Aldrich) for 15 min at room temperature. The samples were observed by spinning disc confocal microscopy with a 100×/1.45 oil objective.

To visualize F-actin fragmentation, F-actin (polymerized from 0.6 μM G-actin) was combined with various concentrations of RIC1 and Ca^{2+} (either 0.6, 0.9, or 1.5 μM RIC1 with 3 μM Ca^{2+} or 1.5 μM RIC1 with 1.5 μM Ca^{2+}) and incubated for 30 min at room temperature. The F-actin was then stained with 0.6 μM Alexa-488 phalloidin for 15 min at room temperature. To disperse actin bundles, 100 mM NaCl was added to the reaction. Samples lacking free Ca^{2+} or RIC1 served as negative controls. The reactions were diluted 10-fold in KMEI buffer prior to observation. The samples were then observed with a spinning disc confocal system (Yokogawa) equipped with an Olympus IX81 microscope and an Andor iXon CCD camera, using a 100×/1.45 oil objective.

To visualize F-actin severing events, a previously reported procedure (Zhang et al. 2010) was adopted with minor modifications. Rhodamine-labeled G-actin was centrifuged at 200,000*g* for 2 h prior to use. Preformed F-actin (polymerized from 0.1 μM rhodamine-labeled G-actin) was added to a flow cell coated with myosin and incubated for 5 min. Then, various combinations of RIC1 and Ca^{2+} were applied to individual flow cells (either 0.05 μM RIC1 with 0, 0.1, 1, 10, or 100 μM free Ca^{2+} or 100 μM free Ca^{2+} with 0, 0.001, 0.005, 0.01, 0.02, 0.05, or 0.1 μM RIC1). The F-actin was immediately observed with a spinning disc confocal microscope using a 100×/1.45 oil objective. Time-lapse images were collected every 5 s for 500 s by TIRFM. The average severing frequency was measured using ImageJ.

To analyze the effects of CA-rop1(G15V) or DN-rop1(T20N) on the F-actin severing ability of RIC1, F-actin (polymerized from 0.6 μM G-actin) was combined with His-RIC1 (0.5 μM), Ca^{2+} (0.15 μM), His-CA-rop1 (0.5 μM), or His-DN-rop1 (0.5 μM) and incubated for 5 min at room temperature. F-actin was then stained with 0.6 μM Alexa-488 phalloidin for 15 min at room temperature. To disperse actin bundles, 100 mM NaCl was added to the reaction solution. Samples lacking RIC1 or rop1 were used as controls. Reactions were diluted 10-fold in KMEI buffer prior to observation. The samples were then observed with a spinning disc confocal microscope equipped with a 100×/1.45 oil objective.

F-actin elongation and depolymerization assays were performed as described previously (Huang et al., 2005; Zhang et al., 2010). For elongation assays, F-actin (polymerized from 0.8 μM G-actin) was incubated with various concentrations of RIC1 (0, 0.4, 0.8, 1.2, and 2 μM) for 5 min at room temperature. After incubation of 1 μM G-actin (10% pyrene-labeled) with 3 μM human profilin I for 2 min on ice, 10× KMEI buffer (15 μL) and G-buffer (5 mM Tris-HCl, pH 8.0, 0.2 mM ATP, 0.5 mM DTT, 0.2 mM $CaCl_2$, and 0.01% NaN_3) were added to initiate elongation at the barbed ends of F-actin filaments. The K_d of RIC1 binding to the barbed ends of actin filaments was determined as described previously (Huang et al., 2003). To test whether the effect of RIC1 on F-actin elongation was Ca^{2+} concentration-dependent, F-actin (polymerized from 0.8 μM G-actin) was incubated with 0.8 μM RIC1 in the presence of various concentrations of free Ca^{2+} (0, 1, 10, and 100 μM). Next, 1 μM G-actin saturated with 3 μM human profilin I was added as described above. The change in fluorescence, indicative of the actin polymerization rate, was monitored using a fluorimeter (QuantaMaster Luminescence QM 3 PH fluorimeter; Photon Technology International) after actin elongation was initiated.

To assay F-actin depolymerization, F-actin (polymerized from 0.2 μM G-actin; 50% pyrene-labeled) was incubated with various concentrations of RIC1 (0, 0.04, 0.08, 0.12, 0.2, 0.28, and 0.4 μM) for 5 min at room temperature. The resulting mixture was then diluted with G-buffer (containing 2 mM EGTA to chelate redundant free Ca^{2+}) until the final volume reached 150 μL. To test whether the effect of RIC1 on F-actin depolymerization was Ca^{2+} concentration-dependent, F-actin (polymerized from 0.2 μM G-actin) was incubated with 0.12 μM RIC1 in the presence of various concentrations of free Ca^{2+} (0, 0.1, 1, 10, and 100 μM). The change in fluorescence, indicative of the actin depolymerization rate, was monitored with a fluorimeter as described above.

Accession Numbers

The sequence data for *RIC1* can be found in the Arabidopsis Genome Initiative database under accession number AT2g33460.

Supplemental Data

Supplemental Figure 1. Analysis of RIC1 Expression Patterns.

Supplemental Figure 2. RIC1 Overexpresssion Reduces Pollen Germination and Pollen Tube Elongation in Vivo.

Supplemental Figure 3. Loss of Function of RIC1 Does Not Affect Microtubule Organization in Pollen Tubes.

Supplemental Figure 4. RIC1 Has No Effect on the Binding of Lifeact to Actin Filaments.

Supplemental Figure 5. RIC1 Affects F-actin Organization in Pollen Tubes.

Supplemental Figure 6. RIC1 Localizes to the Apical Plasma Membrane of Pollen Tubes.

Supplemental Figure 7. RIC1 Bundles Actin Filaments in Vitro.

Supplemental Figure 8. RIC1 Severs F-Actin in the Presence of Ca^{2+} in Vitro.

Supplemental Figure 9. PM-localized RIC1 Oscillates During Pollen Tube Growth.

Supplemental Figure 10. Different Impacts of $RIC1^{H37D/H40D}$ and RIC1 Overexpression on the Organization and Dynamics of Apical F-actin.

Supplemental Figure 11. Effects of ROP1 Activity on RIC1 functioning on F-actin in Vitro.

Supplemental Movie 1. F-actin Dynamics in the Tip of a Growing Col-0 Pollen Tube.

Supplemental Movie 2. F-actin Dynamics in the Tip of a Growing *ric1-1(Col-0)* Pollen Tube.

Supplemental Movie 3. F-actin Dynamics in the tip of a Growing *RIC1 OX 9* Pollen Tube.

Supplemental Movie 4. RIC1 Severs Actin Filaments in the Presence of Ca^{2+} in Vitro.

Supplemental Movie 5. F-actin Dynamics at the Plasma Membrane in the Tip of a Col-0 Pollen Tube.

Supplemental Movie 6. F-actin Dynamics at the Plasma Membrane in the Tip of an *OX 9* Pollen Tube.

Supplemental Movie 7. F-actin Dynamics at the Plasma Membrane in the Tip of a *ric1-1 (Col-0)* Pollen Tube.

Supplemental Movie 8. RIC1-GFP Exhibits Oscillatory Behavior at the PM of Pollen Tube Tips.

Supplemental Movie 9. RIC1-GFP Oscillations at the Plasma Membrane Are Closely Related to Pollen Tube Growth Oscillations.

ACKNOWLEDGMENTS

We thank Ming Yuan (China Agricultural University) for critical comments on the article. We also thank Zhenbiao Yang (University of California, Riverside) for providing the *RIC1*$^{H37D/H40D}$ plasmid and *ric1-1* seeds and for helpful discussions and Chris Staiger and Jiejie Li (Purdue University) for stimulating discussions and advice regarding the analysis of F-actin dynamics. This research was supported by the National Basic Research Program of China (Grant 2012CB114200 to Y.F.) and the Natural Science Foundation of China (Grant 31361140354 to Y.F.).

AUTHOR CONTRIBUTIONS

Y.F. designed the project. Z.Z., H.S., B.C., and R.Z. performed the experiments and analyzed the results. Y.F. wrote the article. Y.F. and S.H. revised and modified the article.

Received December 13, 2014; revised February 13, 2015; accepted March 1, 2015; published March 24, 2015.

REFERENCES

Boavida, L.C., and McCormick, S. (2007). Temperature as a determinant factor for increased and reproducible in vitro pollen germination in *Arabidopsis thaliana*. Plant J. **52:** 570–582.

Bou Daher, F., and Geitmann, A. (2011). Actin is involved in pollen tube tropism through redefining the spatial targeting of secretory vesicles. Traffic **12:** 1537–1551.

Cai, G., Faleri, C., Del Casino, C., Emons, A.M., and Cresti, M. (2011). Distribution of callose synthase, cellulose synthase, and sucrose synthase in tobacco pollen tube is controlled in dissimilar ways by actin filaments and microtubules. Plant Physiol. **155:** 1169–1190.

Cheung, A.Y., and Wu, H.M. (2004). Overexpression of an *Arabidopsis* formin stimulates supernumerary actin cable formation from pollen tube cell membrane. Plant Cell **16:** 257–269.

Cheung, A.Y., and Wu, H.M. (2008). Structural and signaling networks for the polar cell growth machinery in pollen tubes. Annu. Rev. Plant Biol. **59:** 547–572.

Cheung, A.Y., Duan, Q.H., Costa, S.S., de Graaf, B.H., Di Stilio, V.S., Feijo, J., and Wu, H.M. (2008). The dynamic pollen tube cytoskeleton: Live cell studies using actin-binding and microtubule-binding reporter proteins. Mol. Plant **1:** 686–702.

Cheung, A.Y., Niroomand, S., Zou, Y., and Wu, H.M. (2010). A transmembrane formin nucleates subapical actin assembly and controls tip-focused growth in pollen tubes. Proc. Natl. Acad. Sci. USA **107:** 16390–16395.

Choi, Y., Lee, Y., Kim, S.Y., Lee, Y., and Hwang, J.U. (2013). Arabidopsis ROP-interactive CRIB motif-containing protein 1 (RIC1) positively regulates auxin signalling and negatively regulates abscisic acid (ABA) signalling during root development. Plant Cell Environ. **36:** 945–955.

Clough, S.J., and Bent, A.F. (1998). Floral dip: a simplified method for Agrobacterium-mediated transformation of *Arabidopsis thaliana*. Plant J. **16:** 735–743.

Fu, Y., Gu, Y., Zheng, Z., Wasteneys, G., and Yang, Z. (2005). Arabidopsis interdigitating cell growth requires two antagonistic pathways with opposing action on cell morphogenesis. Cell **120:** 687–700.

Fu, Y., Wu, G., and Yang, Z. (2001). Rop GTPase-dependent dynamics of tip-localized F-actin controls tip growth in pollen tubes. J. Cell Biol. **152:** 1019–1032.

Fu, Y., Xu, T., Zhu, L., Wen, M., and Yang, Z. (2009). A ROP GTPase signaling pathway controls cortical microtubule ordering and cell expansion in Arabidopsis. Curr. Biol. **19:** 1827–1832.

Gibbon, B.C., Kovar, D.R., and Staiger, C.J. (1999). Latrunculin B has different effects on pollen germination and tube growth. Plant Cell **11:** 2349–2363.

Gossot, O., and Geitmann, A. (2007). Pollen tube growth: Coping with mechanical obstacles involves the cytoskeleton. Planta **226:** 405–416.

Gu, Y., Fu, Y., Dowd, P., Li, S., Vernoud, V., Gilroy, S., and Yang, Z. (2005). A Rho family GTPase controls actin dynamics and tip growth via two counteracting downstream pathways in pollen tubes. J. Cell Biol. **169:** 127–138.

Higaki, T., Kutsuna, N., Sano, T., Kondo, N., and Hasezawa, S. (2010). Quantification and cluster analysis of actin cytoskeletal structures in plant cells: role of actin bundling in stomatal movement during diurnal cycles in Arabidopsis guard cells. Plant J. **61:** 156–165.

Huang, S., Blanchoin, L., Kovar, D.R., and Staiger, C.J. (2003). Arabidopsis capping protein (AtCP) is a heterodimer that regulates assembly at the barbed ends of actin filaments. J. Biol. Chem. **278:** 44832–44842.

Huang, S., Jin, L., Du, J., Li, H., Zhao, Q., Ou, G., Ao, G., and Yuan, M. (2007). SB401, a pollen-specific protein from Solanum berthaultii, binds to and bundles microtubules and F-actin. Plant J. **51:** 406–418.

Huang, S., Robinson, R.C., Gao, L.Y., Matsumoto, T., Brunet, A., Blanchoin, L., and Staiger, C.J. (2005). *Arabidopsis* VILLIN1 generates actin filament cables that are resistant to depolymerization. Plant Cell **17:** 486–501.

Hussey, P.J., Ketelaar, T., and Deeks, M.J. (2006). Control of the actin cytoskeleton in plant cell growth. Annu. Rev. Plant Biol. **57:** 109–125.

Hwang, J.U., Gu, Y., Lee, Y.J., and Yang, Z. (2005). Oscillatory ROP GTPase activation leads the oscillatory polarized growth of pollen tubes. Mol. Biol. Cell **16:** 5385–5399.

Hwang, J.U., Vernoud, V., Szumlanski, A., Nielsen, E., and Yang, Z. (2008). A tip-localized RhoGAP controls cell polarity by globally inhibiting Rho GTPase at the cell apex. Curr. Biol. **18:** 1907–1916.

Ingouff, M., Fitz Gerald, J.N., Guérin, C., Robert, H., Sørensen, M.B., Van Damme, D., Geelen, D., Blanchoin, L., and Berger, F. (2005). Plant formin AtFH5 is an evolutionarily conserved actin nucleator involved in cytokinesis. Nat. Cell Biol. **7:** 374–380.

Kost, B. (2008). Spatial control of Rho (Rac-Rop) signaling in tip-growing plant cells. Trends Cell Biol. **18:** 119–127.

Kroeger, J.H., Daher, F.B., Grant, M., and Geitmann, A. (2009). Microfilament orientation constrains vesicle flow and spatial distribution in growing pollen tubes. Biophys. J. **97:** 1822–1831.

Kroeger, J.H., Geitmann, A., and Grant, M. (2008). Model for calcium dependent oscillatory growth in pollen tubes. J. Theor. Biol. **253:** 363–374.

Lee, Y.J., Szumlanski, A., Nielsen, E., and Yang, Z. (2008). Rho-GTPase-dependent filamentous actin dynamics coordinate vesicle targeting and exocytosis during tip growth. J. Cell Biol. **181:** 1155–1168.

Li, H., Wu, G., Ware, D., Davis, K.R., and Yang, Z. (1998). Arabidopsis Rho-related GTPases: Differential gene expression in pollen and polar localization in fission yeast. Plant Physiol. **118:** 407–417.

Li, J., Henty-Ridilla, J.L., Huang, S., Wang, X., Blanchoin, L., and Staiger, C.J. (2012). Capping protein modulates the dynamic behavior of actin filaments in response to phosphatidic acid in Arabidopsis. Plant Cell **24:** 3742–3754.

Lin, D., Cao, L., Zhou, Z., Zhu, L., Ehrhardt, D., Yang, Z., and Fu, Y. (2013). Rho GTPase signaling activates microtubule severing to promote microtubule ordering in Arabidopsis. Curr. Biol. **23:** 290–297.

Lin, D., et al. (2012). A ROP GTPase-dependent auxin signaling pathway regulates the subcellular distribution of PIN2 in Arabidopsis roots. Curr. Biol. **22:** 1319–1325.

Michelot, A., Guérin, C., Huang, S., Ingouff, M., Richard, S., Rodiuc, N., Staiger, C.J., and Blanchoin, L. (2005). The formin homology 1 domain modulates the actin nucleation and bundling activity of *Arabidopsis* FORMIN1. Plant Cell **17:** 2296–2313.

Monshausen, G.B., Bibikova, T.N., Weisenseel, M.H., and Gilroy, S. (2009). Ca^{2+} regulates reactive oxygen species production and pH during mechanosensing in *Arabidopsis* roots. Plant Cell **21:** 2341–2356.

Qin, T., Liu, X., Li, J., Sun, J., Song, L., and Mao, T. (2014). Arabidopsis microtubule-destabilizing protein 25 functions in pollen tube growth by severing actin filaments. Plant Cell **26:** 325–339.

Qin, Y., and Yang, Z. (2011). Rapid tip growth: Insights from pollen tubes. Semin. Cell Dev. Biol. **22:** 816–824.

Qu, X., Zhang, H., Xie, Y., Wang, J., Chen, N., and Huang, S. (2013). *Arabidopsis* villins promote actin turnover at pollen tube tips and facilitate the construction of actin collars. Plant Cell **25:** 1803–1817.

Ren, H., and Xiang, Y. (2007). The function of actin-binding proteins in pollen tube growth. Protoplasma **230:** 171–182.

Schiott, M., Romanowsky, S.M., Baekgaard, L., Jakobsen, M.K., Palmgren, M.G., and Harper, J.F. (2004). A plant plasma membrane Ca^{2+} pump is required for normal pollen tube growth and fertilization. Proc. Natl. Acad. Sci. USA **101:** 9502–9507.

Smith, L.G., and Oppenheimer, D.G. (2005). Spatial control of cell expansion by the plant cytoskeleton. Annu. Rev. Cell Dev. Biol. **21:** 271–295.

Staiger, C.J., Poulter, N.S., Henty, J.L., Franklin-Tong, V.E., and Blanchoin, L. (2010). Regulation of actin dynamics by actin-binding proteins in pollen. J. Exp. Bot. **61:** 1969–1986.

Staiger, C.J., Sheahan, M.B., Khurana, P., Wang, X., McCurdy, D.W., and Blanchoin, L. (2009). Actin filament dynamics are dominated by rapid growth and severing activity in the Arabidopsis cortical array. J. Cell Biol. **184:** 269–280.

Vidali, L., Rounds, C.M., Hepler, P.K., and Bezanilla, M. (2009). Lifeact-mEGFP reveals a dynamic apical F-actin network in tip growing plant cells. PLoS ONE **4:** e5744.

Wang, X., Zhu, L., Liu, B., Wang, C., Jin, L., Zhao, Q., and Yuan, M. (2007). *Arabidopsis* MICROTUBULE-ASSOCIATED PROTEIN18 functions in directional cell growth by destabilizing cortical microtubules. Plant Cell **19:** 877–889.

Wu, G., Gu, Y., Li, S., and Yang, Z. (2001). A genome-wide analysis of *Arabidopsis* Rop-interactive CRIB motif-containing proteins that act as Rop GTPase targets. Plant Cell **13:** 2841–2856.

Wu, Y., Yan, J., Zhang, R., Qu, X., Ren, S., Chen, N., and Huang, S. (2010). Arabidopsis FIMBRIN5, an actin bundling factor, is required for pollen germination and pollen tube growth. Plant Cell **22:** 3745–3763.

Yalovsky, S., Bloch, D., Sorek, N., and Kost, B. (2008). Regulation of membrane trafficking, cytoskeleton dynamics, and cell polarity by ROP/RAC GTPases. Plant Physiol. **147:** 1527–1543.

Yokota, E., Tominaga, M., Mabuchi, I., Tsuji, Y., Staiger, C.J., Oiwa, K., and Shimmen, T. (2005). Plant villin, lily P-135-ABP, possesses G-actin binding activity and accelerates the polymerization and depolymerization of actin in a Ca^{2+}-sensitive manner. Plant Cell Physiol. **46:** 1690–1703.

Zhang, H., Qu, X., Bao, C., Khurana, P., Wang, Q., Xie, Y., Zheng, Y., Chen, N., Blanchoin, L., Staiger, C.J., and Huang, S. (2010). *Arabidopsis* VILLIN5, an actin filament bundling and severing protein, is necessary for normal pollen tube growth. Plant Cell **22:** 2749–2767.

Zhu, L., Zhang, Y., Kang, E., Xu, Q., Wang, M., Rui, Y., Liu, B., Yuan, M., and Fu, Y. (2013). MAP18 regulates the direction of pollen tube growth in *Arabidopsis* by modulating F-actin organization. Plant Cell **25:** 851–867.